



**NAVAL
POSTGRADUATE
SCHOOL**

MONTEREY, CALIFORNIA

THESIS

**ATMOSPHERIC EFFECTS ON SIGNAL PROPAGATION
IN ADVERSE ENVIRONMENTAL CONDITIONS: A
VALIDATION OF THE ADVANCED REFRACTIVE
EFFECTS PREDICTION SYSTEM**

by

Erin E. O'Marr

September 2008

Thesis Co-Advisors:

Kenneth Davidson
Karl Pfeiffer

Approved for public release; distribution is unlimited

THIS PAGE INTENTIONALLY LEFT BLANK

REPORT DOCUMENTATION PAGE			<i>Form Approved OMB No. 0704-0188</i>	
Public reporting burden for this collection of information is estimated to average 1 hour per response, including the time for reviewing instruction, searching existing data sources, gathering and maintaining the data needed, and completing and reviewing the collection of information. Send comments regarding this burden estimate or any other aspect of this collection of information, including suggestions for reducing this burden, to Washington headquarters Services, Directorate for Information Operations and Reports, 1215 Jefferson Davis Highway, Suite 1204, Arlington, VA 22202-4302, and to the Office of Management and Budget, Paperwork Reduction Project (0704-0188) Washington DC 20503.				
1. AGENCY USE ONLY (Leave blank)		2. REPORT DATE September 2008	3. REPORT TYPE AND DATES COVERED Master's Thesis	
4. TITLE AND SUBTITLE Atmospheric Effects on Signal Propagation in Adverse Environmental Conditions: A Validation of the Advanced Refractive Effects Prediction System			5. FUNDING NUMBERS	
6. AUTHOR(S) Erin E. O'Marr				
7. PERFORMING ORGANIZATION NAME(S) AND ADDRESS(ES) Naval Postgraduate School Monterey, CA 93943-5000			8. PERFORMING ORGANIZATION REPORT NUMBER	
9. SPONSORING /MONITORING AGENCY NAME(S) AND ADDRESS(ES) N/A			10. SPONSORING/MONITORING AGENCY REPORT NUMBER	
11. SUPPLEMENTARY NOTES The views expressed in this thesis are those of the author and do not reflect the official policy or position of the Department of Defense or the U.S. Government.				
12a. DISTRIBUTION / AVAILABILITY STATEMENT Approved for public release; distribution is unlimited			12b. DISTRIBUTION CODE	
13. ABSTRACT (maximum 200 words) Signal propagation measurements from an 802.16 wireless communications network link were analyzed and compared with respect to effects-based model outputs influenced by atmosphere conditions. Atmospheric data collected included in situ ground measurements, radiosonde upper air observations, and numerical weather model data. Extrapolated vertical atmospheric profiles, based on boundary layer constant flux theory and using the in situ ground measurements, were compared to the radiosonde upper air observations and high resolution numerical weather model data for consistency and accuracy. All three sources of data were input into the Advanced Refractive Effects Prediction System (AREPS) which uses the Advanced Propagation Model (APM) to predict radio frequency (RF) signal loss. AREPS output was compared with measured network signal data. The network studied was part of the COASTS 2007 field experiments in Northern Thailand, a region of highly varied terrain and vegetation as well as adverse environmental conditions. Results validate the extrapolated atmospheric profiles for use as input into tactical decision aids; provide a real-time assessment of the boundary layer and refractive layers overlaid; and compare high resolution numerical model data with radiosonde upper air profiles in the data sparse environment. Results validate AREPS as a Tactical Decision Aid and tool for network administrators and operators for RF signal propagation; determine a negligible statistical significance of refractivity condition impact even though in situ meteorological data captured non-standard refractivity gradients; show that the atmosphere is not a significant contributor to anomalous signal propagation at the operating wavelength and transmission distances; and conclude that the radiation heating of the network equipment remains as the likely factor to impact the transmission signal and equipment.				
14. SUBJECT TERMS 802.16 Wireless Communications Network System, Advanced Refractive Effects Prediction System, Advanced Propagation Model, Boundary Layer Flux Theory, Atmospheric Refractivity, Signal Propagation, COASTS, COAMPS, Radiosonde Upper Air Observations			15. NUMBER OF PAGES 93	
			16. PRICE CODE	
17. SECURITY CLASSIFICATION OF REPORT Unclassified	18. SECURITY CLASSIFICATION OF THIS PAGE Unclassified	19. SECURITY CLASSIFICATION OF ABSTRACT Unclassified	20. LIMITATION OF ABSTRACT UU	

THIS PAGE INTENTIONALLY LEFT BLANK

Approved for public release; distribution is unlimited

**ATMOSPHERIC EFFECTS ON SIGNAL PROPAGATION IN ADVERSE
ENVIRONMENTAL CONDITIONS: A VALIDATION OF THE ADVANCED
REFRACTIVE EFFECTS PREDICTION SYSTEM**

Erin E. O'Marr
Lieutenant, United States Navy
B.S., United States Naval Academy, 2000

Submitted in partial fulfillment of the
requirements for the degree of

**MASTER OF SCIENCE IN METEOROLOGY AND
PHYSICAL OCEANOGRAPHY**

from the

**NAVAL POSTGRADUATE SCHOOL
September 2008**

Author: Erin Elizabeth O'Marr

Approved by: Kenneth Davidson
Co-Advisor

Karl Pfeiffer
Co-Advisor

Philip A. Durkee
Chairman, Department of Meteorology

THIS PAGE INTENTIONALLY LEFT BLANK

ABSTRACT

Signal propagation measurements from an 802.16 wireless communications network link were analyzed and compared with respect to effects-based model outputs influenced by atmosphere conditions. Atmospheric data collected included in situ ground measurements, radiosonde upper air observations, and numerical weather model data. Extrapolated vertical atmospheric profiles, based on boundary layer constant flux theory and using the in situ ground measurements, were compared to the radiosonde upper air observations and high resolution numerical weather model data for consistency and accuracy. All three sources of data were input into the Advanced Refractive Effects Prediction System (AREPS) which uses the Advanced Propagation Model (APM) to predict radio frequency (RF) signal loss. AREPS output was compared with measured network signal data. The network studied was part of the COASTS 2007 field experiments in Northern Thailand, a region of highly varied terrain and vegetation as well as adverse environmental conditions. Results validate the extrapolated atmospheric profiles for use as input into tactical decision aids; provide a real-time assessment of the boundary layer and refractive layers overland; and compare high resolution numerical model data with radiosonde upper air profiles in the data sparse environment. Results validate AREPS as a Tactical Decision Aid and tool for network administrators and operators for RF signal propagation; determine a negligible statistical significance of refractivity condition impact even though in situ meteorological data captured non-standard refractivity gradients; show that the atmosphere is not a significant contributor to anomalous signal propagation at the operating wavelength and transmission distances; and conclude that the radiation heating of the network equipment remains as the likely factor to impact the transmission signal and equipment.

THIS PAGE INTENTIONALLY LEFT BLANK

TABLE OF CONTENTS

I.	INTRODUCTION.....	1
II.	BACKGROUND	5
	A. RADIO WAVE PROPAGATION.....	5
	B. LINE-OF-SIGHT (LOS) SPACE WAVES AND THE ATMOSPHERE	6
	C. REFRACTIVITY.....	6
	D. ADVANCED REFRACTIVE EFFECTS PREDICTION SYSTEM (AREPS).....	11
	E. COOPERATIVE APPLIED SCIENCE AND TECHNOLOGIES STUDIES (COASTS) FIELD EXPERIMENT	13
	F. TELECOMMUNICATIONS AND WIMAX/802.16 STANDARD.....	18
III.	DATA AND METHODOLOGY	21
	A. INTRODUCTION.....	21
	B. RADIO DATA.....	21
	C. METEOROLOGICAL DATA	24
	1. Radiosonde Measurements	24
	2. COAMPS Numerical Weather Model Data	26
	3. Continuous Near-Surface and Ground Measurements.....	27
	4. Data Derived from Application of Surface-layer Similarity Theory	31
	D. PROPAGATION PREDICTIONS.....	33
	E. TERRAIN	33
IV.	RESULTS	35
	A. CHARACTERIZATION OF THE IN SITU ENVIRONMENT	35
	1. March Near-surface Time Series.....	35
	2. May Near-surface Time Series	38
	B. RADIOSONDE AND CAAPS DERIVED SOUNDINGS	41
	1. March Radiosonde and CAAPS Soundings	41
	2. May Radiosonde and CAAPS Soundings	49
	C. RESULTS OF CORRELATION OF METEOROLOGICAL, GROUND MEASUREMENTS AND MEASURED SIGNAL STRENGTH	50
	D. RESULTS WITH EXTRAPOLATED TEMPERATURE, SPECIFIC HUMIDITY, AND MODIFIED REFRACTIVITY PROFILES.....	55
	E. OBSERVED VERSUS OBSERVED SIGNAL DATA	59
V.	DISCUSSION.....	69
	LIST OF REFERENCES.....	73
	INITIAL DISTRIBUTION LIST	75

THIS PAGE INTENTIONALLY LEFT BLANK

LIST OF FIGURES

Figure 1.	AREPS classification of ray geometry for different refractivity conditions. (From Davidson, 2003.).....	8
Figure 2.	Temperature and pressure-height profiles obtained from helicopter measurements in the vicinity of the propagation links, near Wallops Island, Virginia, during an SDF event on 1 April, 1993. (From Goldhirsh et al., 1994.)	9
Figure 3.	Fade time series showing an SDF event (March 14-18, 1990) over the 3-year data collection. March 14-16 segment shown. Note the 60dB SDF 14-15 March. (From Goldhirsh et al., 1994.).....	10
Figure 4.	M-unit relationship for different super-refractive ducting conditions. (From Davidson, 2003.).....	11
Figure 5.	802.16 WiMax/Terrestrial Back Haul Links to Wing-41 and IIFC. (From COASTS CONOPS, 2007)	16
Figure 6.	Google Earth Overhead View of Mae Ngat Dam-METG Area of Operations. (From COASTS CONOPS, 2007).....	17
Figure 7.	Google Earth Overhead View of METG-CHCM Link Area of Operations. (From COASTS CONOPS, 2007)	18
Figure 8.	Example RF Monitor real-time graphic output. (From screen capture during field experiment, 27 Mar 2007.).....	22
Figure 9.	Example SolarWinds SNMP real-time graphic output. (From screen capture during field experiment, 23 May 2007.)	23
Figure 10.	Google Earth Overview of Mae Ngat Dam, Thailand. Note positions of TOC, location site of March ground measurements, and location site of May ground measurements. (Google Earth image, 02 September, 2008.).....	28
Figure 11.	Time series of near-surface meteorological measurements during March test period.....	37
Figure 12.	Time series of the change in refractivity index and modified refractivity index with height during the March test period.....	38
Figure 13.	Time series of near-surface meteorological measurements during May test period.	40
Figure 14.	Time series of the change in refractivity index and modified refractivity index with height during the May test period.	41
Figure 15.	Example M-unit profile from 23 Mar/0100UTC radiosonde launch created using AREPS Environment Creator. Note the low-level subrefraction layer and elevated duct.....	42
Figure 16.	Example M-unit profile from 26 Mar/0100UTC radiosonde launch created using AREPS Environment Creator. Note the low-level trapping.	43
Figure 17.	Example M-unit profile from 26 Mar/0100UTC CAAPS analysis created using AREPS Environment Creator. Note the smoothness of the profile and lack of small feature representation.	44
Figure 18.	27 Mar/0000UTC radiosonde launch sounding. The blue line represents the dewpoint temperature and the red line represents the air temperature.	

	Note the low-level temperature inversion and subsidence aloft. Graphic produced using an MS-DOS PLOTSOND program.....	46
Figure 19.	27 Mar/0000UTC CAAPS analysis field. The blue line represents the dewpoint temperature and the red line represents the air temperature. Note the representative low-level temperature inversion and subsidence aloft. Graphic produced using an MS-DOS PLOTSOND program.....	47
Figure 20.	27 Mar/0000UTC radiosonde Modified refractivity profile. Note the low-level surface duct. Graphic produced using an MS-DOS PLOTSOND program.....	48
Figure 21.	27 Mar/0000UTC CAAPS analysis field Modified refractivity profile. Note the slight representation of a low-level surface duct. Graphic produced using an MS-DOS PLOTSOND program.....	49
Figure 22.	Example of an extrapolated temperature, specific humidity, and M-unit profiles used for analysis. Extrapolation profiles were calculated from averaged 30 minute surface meteorological data on the 23 March from 0000UTC to 0030UTC.	56
Figure 23.	Comparison of M-unit profiles derived from 23 Mar/0100UTC radiosonde launch, CAAPS 23 Mar/0100UTC analysis fields, and 30 min averaged surface meteorological data on 23 March from 0030UTC to 0100UTC.....	57
Figure 24.	Comparison of specific humidity profiles derived from 23 Mar/0100UTC radiosonde launch, CAAPS 23 Mar/0100UTC analysis fields, and 30 min averaged surface meteorological data on 23 March from 0030UTC to 0100UTC.....	58
Figure 25.	Comparison of temperature profiles derived from 23 Mar/0100UTC radiosonde launch, CAAPS 23 Mar/0100UTC analysis fields, and 30 min averaged surface meteorological data on 23 March from 0030UTC to 0100UTC.....	59
Figure 26.	AREPS Communication Editor for building a new communications system within the TDA.....	60
Figure 27.	Extrapolated 23 Mar/0115UTC AREPS M-unit graphic.....	63
Figure 28.	Radiosonde sounding 23 Mar/0100UTC AREPS M-unit graphic.....	64
Figure 29.	CAAPS Analysis 23 Mar/0100UTC AREPS M-unit graphic.	65
Figure 30.	Chiang Mai, Thailand March Climatology AREPS M-unit graphic.	66
Figure 31.	Standard Atmosphere AREPS M-unit graphic.	67

LIST OF TABLES

Table 1.	AREPS classification of ducting characteristics based on refractivity and the Modified M Index values. (From Davidson, 2003).	8
Table 2.	Sample RF Monitor output from field experiment. (From data collected during field experiment, 25 May 2007.)	22
Table 3.	Sample SolarWinds output (From field experiment, 23 May 2007)	23
Table 4.	On-station radiosonde launches Day/UTC Hour and CAAPS analysis and forecast field DAY/UTC Hour.....	25
Table 5.	Selected CAAPS GRIB Fields. Mesh 1 (54 km) at 6-hr intervals, Mesh 2 (18 km) at 6-hr intervals, Mesh 3 (6 km) at 3-hr intervals, and Mesh 4 (2 km) at 1-hr intervals. (From CAAPS FNMOC Request, 09 May 2007.).....	27
Table 6.	Near-surface and ground <i>in situ</i> meteorological set-up and measuring devices.....	29
Table 7.	Correlation table of various atmospheric variables to the measured Received Signal Strength Indicator (received power) during the March testing period.....	52
Table 8.	Correlation table of various atmospheric variables to the measured Received Signal Strength Indicator (received power) during the May testing period.....	53
Table 9.	March received power, air temperature, relative humidity, and specific humidity statistics.	54
Table 10.	May received power, air temperature, relative humidity, and specific humidity statistics.	54
Table 11.	Correlation table of dN/dz and dM/dz to the measured Received Signal Strength Indicator (received power) during the March and May testing periods.....	55
Table 12.	Mean and standard deviation of APM predicted received power (RSSI) and measured signal received power for TOC-METG radio link. March measured RSSI not available.	61
Table 13.	Mean and standard deviation of APM predicted received power (RSSI) and measured signal received power for METG-CHCM radio link.....	61
Table 14.	Mean and standard deviation of APM predicted propagation loss and measured signal link loss for TOC-METG radio link.	62
Table 15.	Height/M-unit comparison for all Meteorological data. Height is in meters.....	68

THIS PAGE INTENTIONALLY LEFT BLANK

LIST OF ABBREVIATIONS AND ACRONYMS

AGL	Above Ground Level
APM	Advance Propagation Model
AREPS	Advanced Refractive Effects Prediction System
C4ISR	Command and Control, Communications Computers and Intelligence, Surveillance and Reconnaissance
CAAPS	Navy's Centralized Atmospheric Analysis and Prediction System
CCIR	International Telecommunication Union, International Radio Consultative Committee
CNO	Chief of Naval Operations
COAMPS	Coupled Ocean Atmosphere Mesoscale Prediction System
COASTS	Cooperative Applied Science and Technologies Studies
CONOPS	Concept of Operations
COTS	Commercial-off-the-shelf
dB	Decibel
dB _i	Decibel Isotropic
dB _m	Power ratio in decibels of the measured power referenced to one milliwatt
DoN	Department of the Navy
DTED	Digital Terrain Elevation Data
EHF	Extremely High Frequency
EM	Electro-Magnetic
ESM	Electronic Countermeasures
FNMOCC	Fleet Numerical Meteorology and Oceanography Center
GHz	Giga-hertz
GPS	Global Positioning System
GRIB	Gridded Binary
Hz	Hertz
IEEE	Institute of Electrical and Electronic Engineers
LF	Low Frequency
LOC	Location

Mb	Mega-byte
MHz	Mega-hertz
MRS	Mini Rawinsonde System
MSL	Mean Sea Level
M-UNIT	Modified Refractivity Units
N	Refractivity Index
NIPRNET	Non-Classified Internet Protocol Router Network
OFDM	Orthogonal Frequency-Division Multiplexing
RF	Radio Frequency
RMS	Root Mean Square
RSSI	Received Signal Strength Indicator
SHF	Super High Frequency
SINADR	Signal to Noise and Distortion Ratio
SNMP	Simple Network Management Protocol
SNR	Signal-to-Noise Ratio
SPAWAR	Space and Naval Systems Warfare Command
SRTM	Shuttle RADAR Topography Mission
TDA	Tactical Decision Aid
TNT FE	Tactical Network Topology Field Experiment
TOC	Tactical Operations Center
UAV	Unmanned Aerial Vehicle
USGS	U.S. Geological Survey
VWC	Volumetric Water Content
WGS	World Geodetic System
WIMAX	Worldwide Interoperability for Microwave Access

ACKNOWLEDGMENTS

I would like to acknowledge and express gratitude to the following people:

— Dr. Ken Davidson and LtCol Karl Pfeiffer for their patience, time and expertise.

— Mr. Richard Lind for his Meteorological and Environment Science expertise. Also for building the meteorological system enabling data collection during research.

— Ms. Mary Jordon for her time and expertise in MATLAB. You helped to bring my ideas to fruition.

— Mrs. Tamar Neta for her MATLAB codes and recommendations.

— Ms. Amalia Barrios for her time and guidance throughout experimentation and research.

— SPAWAR San Diego and PMW-180 for travel and equipment funding.

— FNMOC Monterey, California for selected COAMPS model runs and fields imperative for this research.

— The COASTS 2007 students, faculty, reservists, and contractors.

— NIOC Suitland for guidance of data and methodology.

THIS PAGE INTENTIONALLY LEFT BLANK

I. INTRODUCTION

Information superiority plays a vital role in determining decisive victory during engagement with an adversary. Fast, deployable and scalable communications networks provide real-time situational awareness to operators, especially in rural areas where no land-line, permanent infrastructure exists.

The following research is guided by two separate but equally important purposes. The first is to assess the application of the Advanced Propagation Model (APM) over land for super high frequency (SHF) communications. APM, developed by the Space and Naval Systems Warfare Command, San Diego (SPAWAR SSC, San Diego), was originally designed for predicting radar propagation loss over water. Over the past decade, SPAWAR has been extending APM for estimating propagation loss within the coastal region and over land. In addition to extending APM to different environmental conditions, this study re-examines previous research regarding atmospheric impacts on propagation loss in 5.8 gigahertz (GHz) wireless networks. The focus of this work is on collection and analysis of field data, primarily in the form of concurrent *in situ* network connectivity measurements and robust *in situ* meteorological measurements, and also meso-scale predictions by numerical models. Both research goals further our understanding of wireless networking in tactical and operational situations across adverse environments with varied vegetation and terrain.

According to Barrios et al. (2006), the APM, a propagation model used within SPAWAR's Advanced Refractive Effects Prediction System (AREPS) effects model tactical decision aid (TDA), has been proven and tested viable since its development for over water use in the 1970s; followed by testing and validation for over land and near coastal use occurring over the past decade. Not only do most propagation data collection studies over land focus on terrain effects and not direct atmospheric effects with corresponding meteorological measurements, but most of the propagation models neglect vertical and horizontal changes in refractivity gradients (Barrios et al., 2006). Barrios et al. (2006) also describes APM use of a hybrid ray optics/parabolic equation model in

order to include the atmospheric and environmental inhomogeneity often found in communication system operational areas.

Miller (2006) completed a statistical analysis of wireless networking for predicting performance in multiple environmental conditions. He found a direct correlation between decreasing throughput and increasing atmospheric humidity. Specifically, Miller found a decrease of 0.347 Mega-byte (Mb) throughput for each corresponding percentage point increase in atmospheric humidity (Miller, 2006). Miller further concludes humidity, in isolation, provides an adequate linear model for predicted throughput. A purpose of this thesis is to explore whether a physical versus statistical relationship existed between throughput and values of one atmosphere variable. It is believed that if a relationship existed it would be with a derived property, such as the gradient of humidity.

Theoretically, atmospheric affects on the 5.8 GHz wavelength from either scattering in the presence of moisture or gaseous absorption should be minimal (Davidson, 2003). The wavelength is appreciably longer than impinging water droplets and/or particulate matter. Temperature and humidity may not be individually important, but together the vertical gradients are effectual components of the electromagnetic index of refraction. A focal point of this research takes into consideration the change of temperature and of specific humidity with height and identifies the presence of non-standard refractivity gradients. Refractive effects do not depend on the wavelength versus constituent sizes. However, wavelength can be a factor if atmosphere waveguides are factors. Refractivity conditions do affect SHF frequencies (Davidson, 2003). Subrefractive and super-refractive conditions can cause a shortening or lengthening of transmission and detection ranges, respectively. Super-refraction can cause changes of the position of nulls formed by direct and surface reflection indirect rays.

This thesis addresses the impact of *in situ* atmospheric conditions surrounding the wireless network access points; explores the refractive conditions; and correlates corresponding transmitter/receiver power and propagation loss/link loss measurements. Field experiments took place in northern Thailand during the months of March and May/June. Timing of the field experiments enables the research to explore differing

climatological conditions. The March testing period takes place during the Northeast (NE) Monsoon season. During the NE Monsoon, a Siberian high pressure system brings relatively colder, drier air from the north over the region of study. The May-June testing period occurs during Southeast Asia's transition to the Southwest (SW) monsoon. The SW monsoon regime brings relatively warmer, moister air from the south (Bay of Bengal and Indian Ocean) into the region of study. The analysis also uses both *in situ* meteorological measurements and forecasted numerical weather model atmospheric profiles as input into APM. The output predictions are compared with measured signal data. Lastly, the research includes the usefulness and potential limitations of AREPS as a tactical decision aid for over land performance of SHF communications systems.

This thesis is organized as follows: Chapter II provides a brief background on signal propagation and atmospheric effects; Chapter III describes the data collection methodology and provides a short background on the field experiments conducted in COASTS 2007; Chapter IV examines the network and possible impact of atmospheric effects based on data collected, with emphasis on statistically significant and physically meaningful results; and Chapter V summarizes this work with recommendations for future directions in this research.

THIS PAGE INTENTIONALLY LEFT BLANK

II. BACKGROUND

A. RADIO WAVE PROPAGATION

Radio frequency signal propagation occurs with orthogonal electromagnetic (EM) fields transmitting through a dielectric free space medium. The radiated EM fields undergo spherical spreading as the wavefront propagates from the transmitter to the receiver. The transmitted power and intensity decrease with distance away from the transmitting source as a result of the spherical spreading. The signal strength further decreases or can be increased over distance as a result of reflection from the surface, atmosphere refraction, and diffraction past obstacles as it interacts with the atmosphere and environment (Davidson, 2003). Description of anomalous propagation of microwave radiation started as early as the 1930's, as described by Babin (1995). Most interactions between an EM signal and the environment are frequency (wavelength) dependent.

Diffraction is a result of the EM wavefront bending around an obstacle in its propagation path between the transmitter and receiver. Diffraction often results in multipath propagation where the received signal arrives, simultaneously, by different paths. This constructive/destructive interference cancels, fades, and/or enhances the signal.

Refraction causes the bending of the EM wave geometry through scattering incident to the wavefront. Refraction of the EM wavefront directly relates to the index of refraction gradient within the propagating medium and results in the effective phase change (slight retardation) of the wave. The index of refraction, n , is calculated as a ratio between the phase velocity in a vacuum, c , and the phase velocity in the medium, v .

$$n = c / v \tag{1}$$

In the troposphere, the index of refraction decreases with height which effectively bends the EM wavefront back toward the earth. EM waves bend toward the region(s) of slower wave-front phase speed (higher index of refraction) (Davidson, 2003).

B. LINE-OF-SIGHT (LOS) SPACE WAVES AND THE ATMOSPHERE

The SHF wavelengths are primarily affected through atmospheric refraction caused by the vertical variation (gradient) of pressure, temperature, and humidity along the path (Burk & Thompson, 1996). The density variation results in different phase velocities of the medium which affects the index of refraction. The gradient of the index of refraction, dn/dz , describes the resultant “bending” or curvature of the wavefront of transmission within its given environment. The impact of water vapor molecules within the atmosphere is most significant (Davidson, 2003).

The vertical gradient of refractivity creates trapping layers and associated ducts or wave guides that trap and guide the EM wavefront between the transmitter and receiver. Meteorological vertical profile measurements collected using radiosonde and direct surface measurements, help to understand and characterize the atmosphere between the transmitter and receiver.

C. REFRACTIVITY

The index of refraction is a function of atmospheric pressure, temperature, and water vapor. The dimensionless refractivity index, N , is defined as

$$N = 10^6(n - 1) \quad (2)$$

where as, the gradient of refractivity is defined as

$$\frac{dN}{dz} = \frac{dn}{dz} \cdot 10^6 \quad (3)$$

Predictions of microwave propagation requires height profiles of dN/dz , where the slope change characterizes the propagation as normal, super-refractive, subrefractive, or falling within a trapping environment (Babin, 1995). Davidson (2003) presents the following expression:

$$N = 77.6 \cdot \left(\frac{P}{T}\right) - 5.6 \cdot \left(\frac{e}{T}\right) + 3.75 \cdot \left(10^5 \times \frac{e}{T^2}\right) \quad (4)$$

where P = pressure (mb), T = temperature (K), e = water vapor (mb) (Davidson, 2003). From equation (4), refractivity is therefore directly proportional to pressure and water

vapor, and inversely proportional to temperature. In a standard atmosphere ($P = 1013$ mb, $T = 288$ K, and $e = 20$ mb), $dN/dz \sim -40 \text{ km}^{-1}$. When the refractivity gradient is positive, $dN/dz > 0 \text{ km}^{-1}$, microwave radiation is refracted upward relative to the line of sight, or geometric. This could mean that a receiver within the horizon would not receive the signal (Davidson, 2003).

Babin (1995) emphasizes and describes propagation evidence that in a ducting environment, where the microwave radiation is diffracted towards the earth in a wave guide:

$$\frac{dN}{dz} \leq -157 \text{ km}^{-1} \quad (5)$$

Because this gradient is associated with a wave guide, relative to earth's surface, frequency dependence is associated with the impact. The impact of the waveguide is inversely proportional to the frequencies, i.e. higher frequencies are influenced more than lower frequencies.

In addition to refractivity (N), another commonly used modified index M-units, is used to depict refractive conditions, the existence of various ducting layers, and the resulting ray geometry. The modified M-unit index is very useful in determining the presence of trapping conditions with associated duct or waveguides. M-units are defined as:

$$M = N(z) + 157z \quad (6)$$

where $N(z)$ is the value of refractivity at height z and the height in the atmosphere, z , is in kilometers. M increases with height in a standard atmosphere. Therefore, if M has a negative gradient, followed by a positive gradient, a trapping layer with associated duct occurs with the top of the duct being the top of the trapping layer, or at the level where the M gradient changes from negative to positive (Davidson, 2003).

Table 1 includes AREPS classification for all refractive conditions. Figure 1 depicts the ray geometry for different refractive conditions, for a surface transmitted over

the sea. The same scene for a land based transmitter would have topography. Both illuminate the usefulness of the modified M refractive index. M-units are considered and used throughout the remaining text.

Table 1. AREPS classification of ducting characteristics based on refractivity and the Modified M Index values. (From Davidson, 2003).

IREPS Classification	$\frac{dN}{dZ}$	$\frac{dM}{dZ}$	Distance to Surface Horizon
Subrefraction	$>0 \text{ km}^{-1}$		Reduced
Normal	0 to -79 km^{-1}	$>157 \text{ km}^{-1}$	Normal
Superrefraction	-79 km^{-1} to 157 km^{-1}	0 to 79 km^{-1}	Increased
Trapping	$<-157 \text{ km}^{-1}$	$<0 \text{ km}^{-1}$	Greatly increased

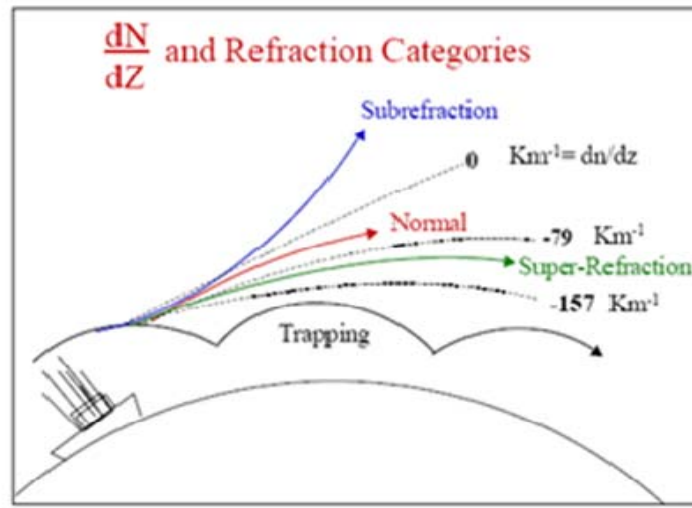


Figure 1. AREPS classification of ray geometry for different refractivity conditions. (From Davidson, 2003.)

SUBREFRACTIVE: As described above, an RF ray will bend upward relative to the geometric and cause Table 1 indicated reduced ranges due to shorter horizon. According to Eqn (4), subrefraction will be associated with humidity increasing or temperature decreasing with heights. Calculations with representative atmosphere values of all variables are necessary to establish the occurrence of subrefraction. Subrefractive conditions are likely over tropical land, as in the test region, if horizontal advection of humidity occurs, or due to afternoon radiative heating of surface. A synoptic driven situation in which a fade of 60 dB over an overwater path of ~ 22 nm (~41 km) was

described for C-band (4.7 GHz) by Goldhirsh, Dockery, and Myer (1994). In that case, warm moist air flowing over cool water surface, led to the refractivity profile and signal strength measurements shown in the following figures, respectively. The sustained deep fade (SDF) events with 60 dB fades occurred during these episodes. Figure 2 shows the refractivity profile (calculated from measurements of the total pressure, temperature, and water vapor pressure) corresponding to an SDF event on 1 April, 1993. Figure 3 shows the power fade relative to free space power that can occur during an SDF event.

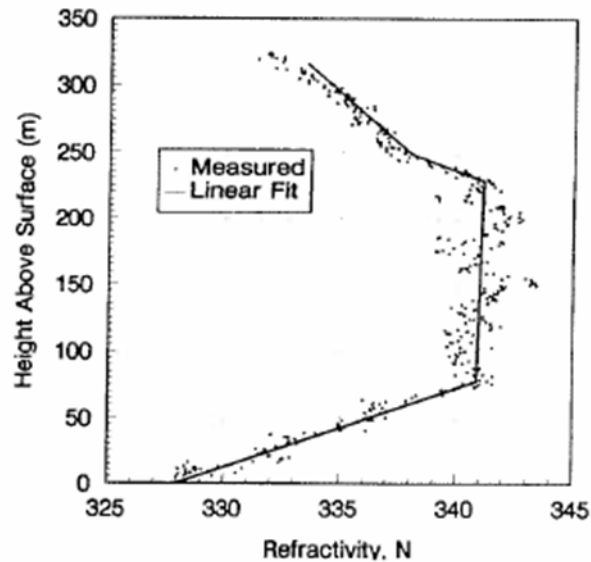


Figure 2. Temperature and pressure-height profiles obtained from helicopter measurements in the vicinity of the propagation links, near Wallops Island, Virginia, during an SDF event on 1 April, 1993. (From Goldhirsh et al., 1994.)

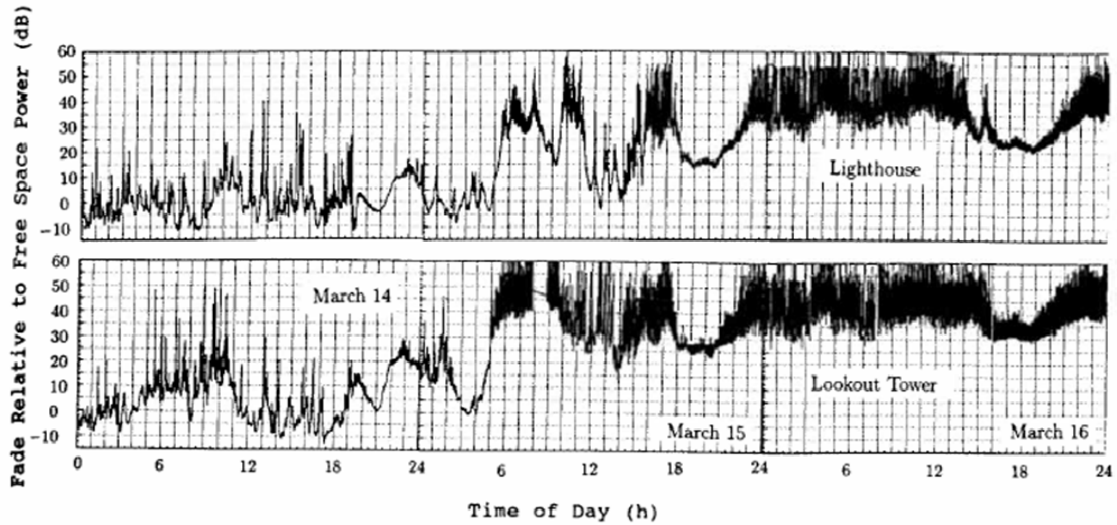


Figure 3. Fade time series showing an SDF event (March 14-18, 1990) over the 3-year data collection. March 14-16 segment shown. Note the 60dB SDF 14-15 March. (From Goldhirsh et al., 1994.)

SUPER-REFRACTIVE: As described above, trapping layers with associated ducting conditions channel the EM energy, i.e., a wave-guide. Trapping occurs when $dM/dz < 0$ and in response, EM rays bend downward toward the earth. Positive temperature gradients (rapid increase in temperature with height) and negative humidity gradients (rapid decrease in humidity with height) above the surface both result in a negative M gradient. Ducting layers “trap” EM energy between the bottom and top if the transmitter is located within it. The top of a duct coincides with the top of a trapping layer; however, the bottom of a duct can extend below the bottom of a trapping layer (Davidson, 2003). Atkinson et al. (2000) describe the five basic processes that lead to duct formation including: rapid evaporation over the sea, subsidence in the presence of an anticyclone, subsidence along a frontal surface, nocturnal radiative cooling over land, or advection.

There are three different types of ducts: elevated, surface-based, and surface-trapping. An elevated duct does not extend to the surface. A surface-based duct extends from the top of the trapping layer to the surface. The surface trapping, or evaporation over water duct is a thin-layered duct, with its base at the surface that results from a rapid

increase in temperature and/or decrease in humidity leading to $\frac{dN}{dz} \leq -157\text{km}^{-1}$ immediately above the surface (Davidson, 2003). Relative to ducting, this paper also addresses the existence of surface-based and elevated ducts and their affect on microwave communications over land. The transmission range would influence the importance of these conditions occurring. Figure 4 illustrates the three types of ducting conditions using the M-unit profile.

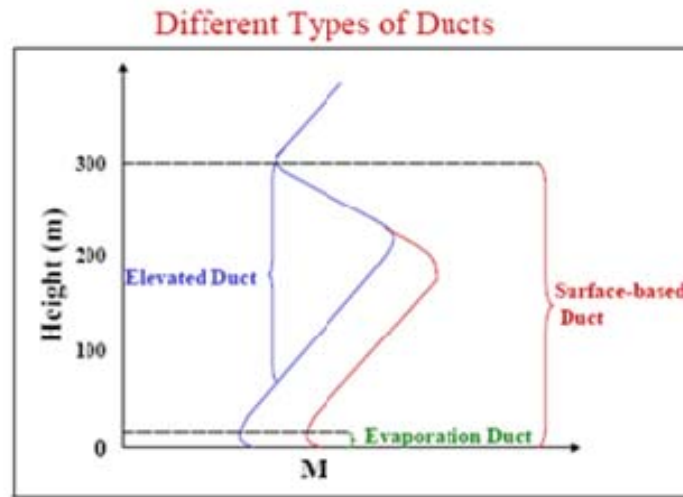


Figure 4. M-unit relationship for different super-refractive ducting conditions. (From Davidson, 2003.)

D. ADVANCED REFRACTIVE EFFECTS PREDICTION SYSTEM (AREPS)

An operational propagation model (APM) and an effects model (AREPS) were used to evaluate possible atmosphere impacts on the transmission. AREPS is an approved EM system assessment application with the Department of the Navy (DoN) Chief Information Officer, DoN Applications and Database Management System (DADMS). It was developed by the Atmospheric Propagation Branch of Space and Naval Warfare System Center, San Diego (Patterson, 2007). Operators use AREPS as a tactical decision aid (TDA) graphical user interface to assess the range and bearing dependent environmental impacts on a particular end-to-end EM system. EM systems include LF-EHF communications, electronic countermeasures (ESM), ESM vulnerability,

and radar. AREPS includes free space transmission, multipath interference, diffraction, tropospheric scatter, subrefraction, super-refraction, and trapping over sea and/or terrain paths. It includes sea surface and terrain clutter, as well as the absorption of EM energy by oxygen and water vapor (Patterson, 2007). The impact of the *in situ* atmosphere on microwave EM is the subject of this study.

For specified EM transmission and receiving systems, AREPS displays the predicted propagation loss, received power, and signal-to-noise ratio versus range and height. It derives its terrain data from Digital Terrain Elevation Data (DTED) or Shuttle Radar Topography Mission (SRTM) data. AREPS also includes various surface type conditions, as defined by the International Telecommunication Union, International Radio Consultative Committee (CCIR), which is especially necessary when operating with vertically polarized antennas (subject of this study). AREPS accepts atmospheric data in the form of *in situ* observations and/or radiosonde profiles, numerical weather models fields, or its built-in climatological databases. AREPS takes the ingested atmospheric data and produces a height versus Modified refractivity profile required by the internal propagation models (Patterson, 2007).

AREPS uses various propagation models to model the range and height dependent propagation over both water and terrain through split-step or finite-difference parabolic equations (SSC Branch Overview, 2005). It uses the Advanced Propagation Model (APM) for frequencies between 2 and 57 GHz (Statement of Functionality, 2006). The APM is the only Chief of Naval Operations (CNO) accredited EM propagation model for use with U.S. Navy systems. Barrios (2003) further describes the hybrid (ray-optics and parabolic equation) APM and the various approximations used.

AREPS has various subroutines which enable the user to create a new project to model, to create the environmental input for APM, and to build/specify the operating communications system. The Environment Creator can import World Meteorological Organization messages, use atmospheric information from an upper air or surface climatological databases, or allow the user to custom import and create an environment for APM input using *in situ* atmospheric measurements. The Communications Editor allows the user to build and define a specific communications platform to model within

AREPS. The AREPS new project screen allows the user to build a specific decision aid (Radar detection, ESM vulnerability, Communications), define the environment to use (atmosphere, terrain, and wind), define the graphic display (height and range), specify the system (platform and target; receiver and transmitter), and define the project geographic area (latitude, longitude, and bearings).

AREPS has been evaluated for overland use by its developers. Barrios et al. (2006) conducted an APM validation study for low altitude signal propagation over land with a mobile receiver and varying signal propagation distances. Barrios et al. (2006) found up to a 29.9 dBm APM RMS error between the predicted and observed. They also concluded that refractivity conditions had “little effect of statistical significance” and that terrain resolution and elevation had a greater effect.

E. COOPERATIVE APPLIED SCIENCE AND TECHNOLOGIES STUDIES (COASTS) FIELD EXPERIMENT

The COASTS field experiment program is a combined U.S.-Indonesia-Malaysia-Singapore-Thailand Research and Development (R&D) effort exploring the use and application of Commercial-off-the-shelf (COTS) Command and Control, Communications Computers and Intelligence, Surveillance and Reconnaissance (C4ISR) technologies for multi-national, cooperative use within tactical and operational situations. There is an increasing and immediate requirement for low-cost, state-of-the-art, real-time, mobile threat warning and tactical communication equipment that can be rapidly deployed, is scalable, and can be formed around operational needs and considerations. The principal COASTS 2007 technologies include:

- Wireless network communications systems
- Simple Network Management Protocol (SNMP) based multi-sensor networking devices
- Networked sensors
- Biometric systems
- UAVs (fixed and rotary wings)
- Tethered balloons
- Portable computing systems

- C4I software applications
- Deployable meteorological sensor suites
- Information management portals

COASTS 2007 conducted three in-country field experiments and one out-of-country Thailand field experiment as a precursor to the annual capstone field experiment (May and June) at the Mae Ngat Dam north of Chiang Mai, Thailand.

COASTS R&D programmatic concept stems from the Tactical Network Topology Field Experiment (TNT FE), another Naval Postgraduate School-led field experiment active since FY2002. Whereas TNT FE addresses Classified systems, COASTS activated to address global interoperability and expand our R&D efforts with foreign military partners to improve command and control between friendly assets, disadvantaged users, and tactical units. Specific, but not inclusive, COASTS-07 objectives include:

- Investigate net-centric information management in a multi-national environment across tactical, operational, and strategic domains
- Make ISR data and information visible, available and usable when and where needed
- Investigate deployment issues surrounding hastily formed networks in rugged and varied terrain under adverse climatic conditions

Wireless network components and technologies demonstrated included:

- Mesh Dynamics 802.11 wireless mesh network components
- Redline Communications 802.16 network components
- Motorola/Orthogon 802.16 components
- Fortress Technologies 802.11 and 802.16 secured wireless mesh network components

This study used signals of opportunity from the Redline Communications and Motorola/Orthogon 802.16 network components. The Redline AN-50e 802.16 Orthogonal Frequency-Division Multiplexing (OFDM) wireless Point-to-Point communication suite uses a 2x2 foot parabolic flat panel antenna with data throughput rates up to 54 Mbps. The radio transceivers have a range of up to 30-km with negligible

latency and jitter problems. Motorola/Orthogonal 802.16 network components, using the Motorola 400 Series Point-to-Point, Multiple-Input Multiple Output 5.4 GHz and 5.8 GHz wireless Ethernet bridges combine OFDM with advanced signal processing algorithms for even higher aggregate throughput rates (COASTS CONOPS 2007). Both flat panel antennas are vertically polarized. Vertical polarization defines the orientation of the radio waves as perpendicular to the Earth's surface as they radiate from the antenna (Alexander, 2005).

Field measurements were taken at the first two relay links from the Tactical Operations Center (TOC) at the Mae Ngat Dam, of the COASTS 2007 802.16 WiMax/Terrestrial Back Haul Links (Figure 5). Motorola/Orthogon equipment transmits from the Mae Ngat Dam (LOC: 19 09'45.10N, 99 02'21.00E) to METG (LOC: 19 07'05.88N, 98 57'16.92E) antenna towers. The link is 10.15-km long with a true bearing of 61.13 degrees. Varied terrain and vegetation exists (Figure 6). Redline equipment transmits between the METG and CHCM (LOC: 18 51'58.64N, 98 58'04.30E) antenna towers. The link extends 27.93-km at a true bearing of 357.16 degrees. Varied terrain and vegetation exists (Figure 7). Network topology, as defined in the COASTS 2007 Concept of Operations (CONOPS) integrates all disparate technologies, wirelessly, into a common operating picture; transmits the collected information via the terrestrial back haul (relay) links; and subsequently, delivers situation awareness to distant commanders in Bangkok, Thailand, and Monterey, California, via satellite communications (COASTS CONOPS, 2007).

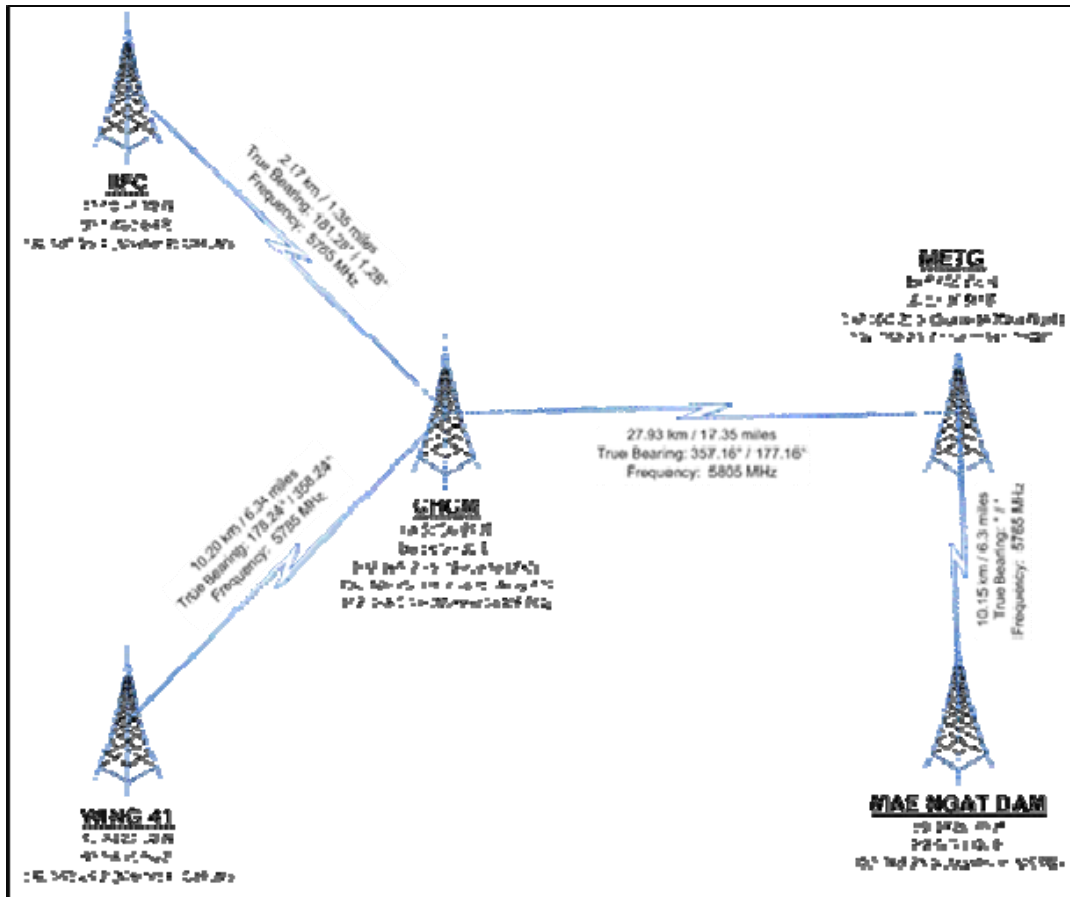


Figure 5. 802.16 WiMax/Terrestrial Back Haul Links to Wing-41 and IIFC.
 (From COASTS CONOPS, 2007)



Figure 6. Google Earth Overhead View of Mae Ngat Dam-METG Area of Operations.
(From COASTS CONOPS, 2007)

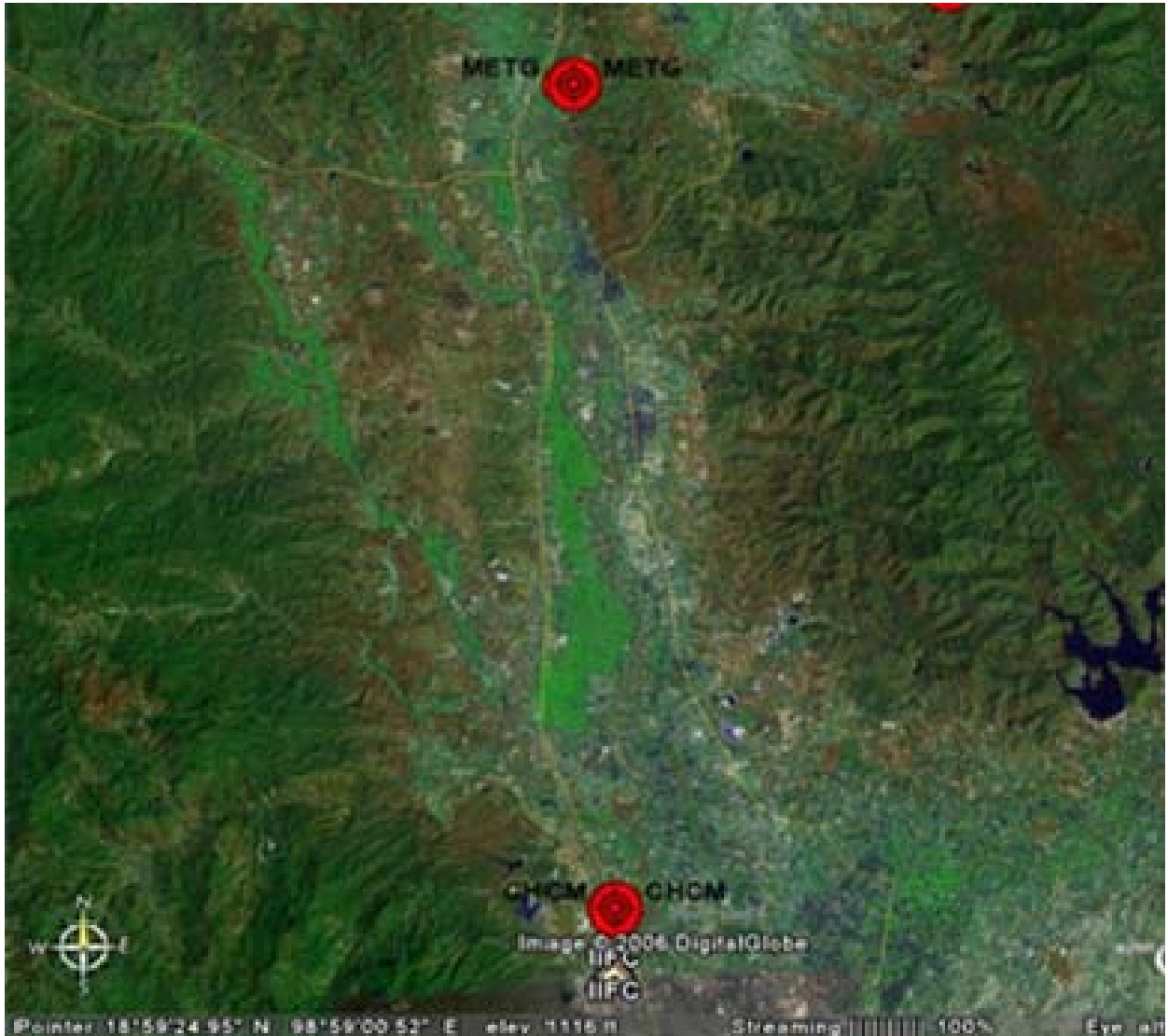


Figure 7. Google Earth Overhead View of METG-CHCM Link Area of Operations.
(From COASTS CONOPS, 2007)

F. TELECOMMUNICATIONS AND WIMAX/802.16 STANDARD

The basic definition of telecommunications is: communications at a distance (Freeman, 1998). The field experiment uses 802.16 protocols, or the Worldwide Interoperability for Microwave Access (WiMax) as described in the previous section. The Institute of Electrical and Electronic Engineers (IEEE), a national standardization organization, defines the 802 series specifications. The 802.16 standard breaks the electromagnetic spectrum up into two sections: 2-11 GHz and 11-66 GHz (Moltzan,

2005). The defined protocol provides network users with standardized procedures to initiate transmission; acknowledge, receive, and assimilate packets; and terminate the session (Thompson et al., 2006). The 4-6 GHz bands have an available bandwidth of up to 500 mega-hertz (MHz), allocated between 20 and 30 MHz segments for subcarriers (Freeman, 1999).

The transmitter, using OFDM, uses multiple orthogonal subcarriers at different frequencies to sustain high availability. Each of the subcarriers transmit the information at a particular bandwidth, on overlapping frequencies, for a rate of "x" per second (Thompson et al., 2006). The multiple signals, at different frequencies, have greater resistance in multipath environments for protection against severe multipath fading (Alexander, 2005). The robust modulation scheme effects a 99.999 percent link availability (Moltzan, 2005). LOS microwave transmits over a single link or a series of links (as described by the present experiment).

As Freeman (1998) defines, network administrators follow several steps in link engineering:

- Selection of sites (radio equipment plus tower locations)
- Selection of operational frequency band from those set forth (commercially used), considering RF interference environment and legal restraints
- Development of path profiles to determine radio tower heights
- Link path calculation- the received signal must be above a threshold level
- Conduct a path survey
- Establish a frequency allocation plan
- Configure all equipment
- Install requisite equipment
- Beam alignment and equipment lineup

The evaluation of the propagation path and determination of Fresnel Zone clearance are important for LOS microwave radio wave links. Link loss will occur as the signal wavefront expands and travels through atmospheric medium (as described in previous sections). Empirically, wavefront clearance must exceed 0.6 of the first Fresnel

Zone radius. Excess attenuation will occur as the signal travel across varied vegetation. If the resultant attenuation becomes too large, diffraction could be a possibility and must be considered (Freeman, 1998).

III. DATA AND METHODOLOGY

A. INTRODUCTION

In this chapter, radio and meteorology data collection strategy and implementation are presented. The study was carried out as collaborating participants with the radio-based field campaign, and directing participants with the field-based collection, and production facility numerical prediction. The planned approach was intended to maximize the collection of radio propagation data coincident in time and space with meteorological boundary layer data. In addition to the in situ atmospheric data, model fields independent of these data were gathered post-field experiment from operational numerical products. Finally, analytic models based on similarity theory were used to further extend the usefulness of field data from radiosonde and surface collections.

B. RADIO DATA

The super high frequency (SHF) signals of opportunity were from Redline Communications and Motorola 802.16 network components as discussed in Chapter II. Testing occurred approximately 40 km north of Chiang Mai, Thailand, at the Mae Ngat Dam. The Redline Communications suite includes a web interface RF Monitor tool, downloadable to a laptop computer, which automatically polls the web interface for received signal strength indicator (RSSI) in dBm (equivalent to received power), signal to noise and distortion ratio (SINADR) in dB, and transmitted power in dBm. The tool logged and plotted the data twice per second. Moltzan (2005) describes Redline Equipment and RF Monitor in detail. Figure 8 and Table 2 provide an example of the RF Monitor data logger and graphical display.

SolarWinds licensed network management software was used to measure and record the Motorola performance data. The Simple Network Management Protocol (SNMP) tool accessed the Motorola devices, in real-time, for the data collection and graphing of transmit and received power in dBm, link loss expressed in tenths of dB, and signal to noise ratio expressed in tenths of dB. Information on SolarWinds Network

Management tools is found at: <http://www.solarwinds.com/>. Figure 9 and Table 3 provide an example of SNMP data logger and real-time graphical display.

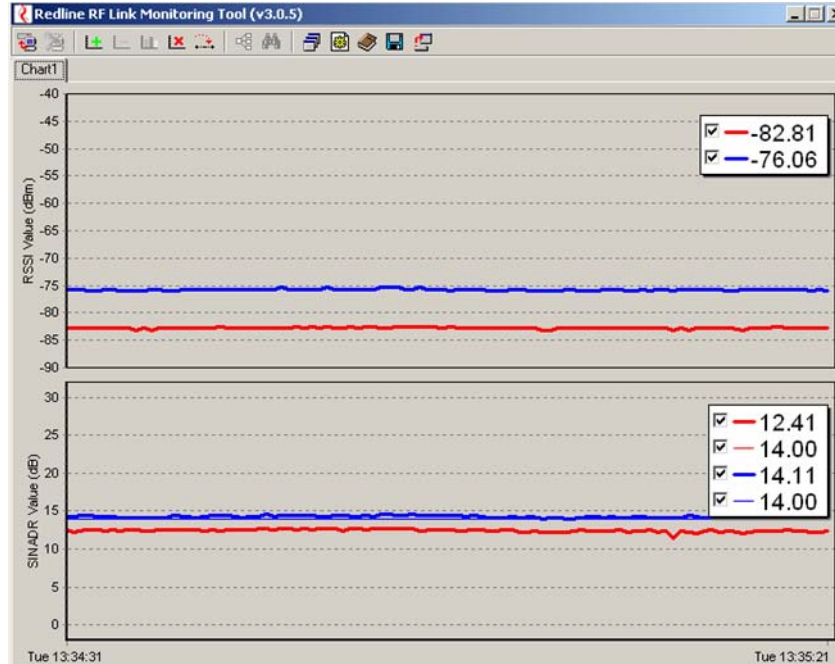


Figure 8. Example RF Monitor real-time graphic output. (From screen capture during field experiment, 27 Mar 2007.)

Table 2. Sample RF Monitor output from field experiment. (From data collected during field experiment, 25 May 2007.)

primaryTimeIndex	primaryRSSI	primarySINDAR	primaryTx
05/25/07 - 09:54:07.562	-82.44	12.21	14

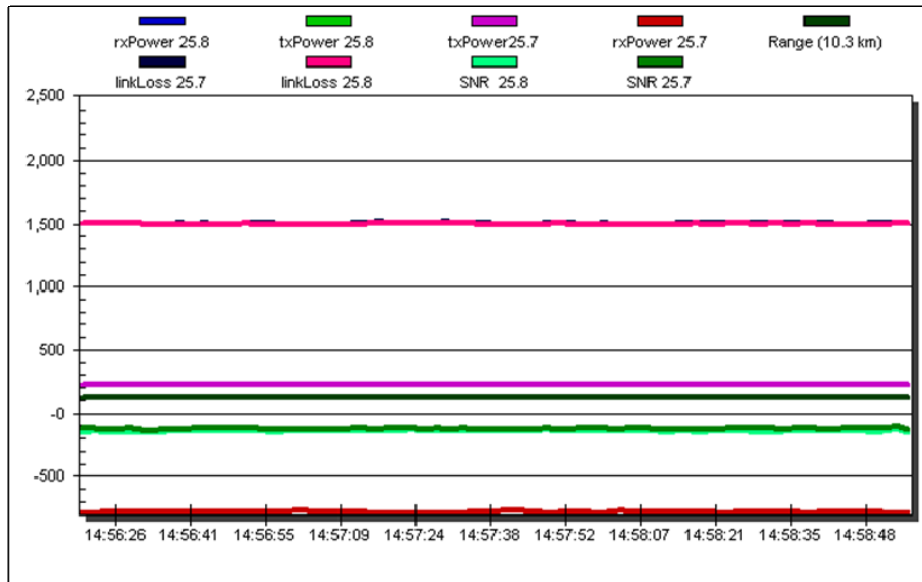


Figure 9. Example SolarWinds SNMP real-time graphic output. (From screen capture during field experiment, 23 May 2007.)

Table 3. Sample SolarWinds output. (From field experiment, 23 May 2007.)

TimeStamp	rxPower 25.8	txPower 25.8	txPower25.7	rxPower 25.7	Range (10.3 km)	linkLoss 25.7	linkLoss 25.8	SNR 25.8	SNR 25.7
02:59:57 PM	-797	210	210	-801	103	1479.00	1,477.00	-169	-151

The SHF signal data were recorded at pre-defined intervals using both RF Monitor and SolarWinds SNMP on their respective communications suites. All necessary calibration was conducted by the network administrators during installation of the communication systems, set-up of monitoring equipment, and initialization of monitoring software. Input power levels and experiment data flow was pre-determined by the network administrators and COASTS Program Manager and in accordance with COASTS 2007 CONOPS and field experiment requirements.

The RF Monitor samples, taken twice per second, were averaged to one-minute intervals in order to merge with ground *in situ* meteorological data. The Redline Link Budget Tool was used to determine system assumptions, biases, and set-up of the Redline communications suite within AREPS. The Redline antenna was assumed to contribute a 28 dBi gain based on the manufacturer’s specifications. Receiver sensitivity was

assumed to be -91 dBm. Assumed implementation system loss was 6 dB. Transmit frequency was 5.8 GHz with a bandwidth of 10,000 Hz (max allowable in AREPS).

Antenna type input was $\frac{\sin x}{x}$ with vertical polarization and vertical beam width of 6 degrees.

SolarWinds SNMP samples were taken between one and 10 minute intervals. The Motorola Point-to-Point Link Estimator Configuration Worksheet was used to determine system assumption, biases, and set-up of the Motorola communications suite within AREPS. The Motorola antenna was also assumed to contribute a 28 dBi gain. Receiver sensitivity was assumed to be -91 dBm. Assumed implementation system loss was 0.86 dB. Transmit frequency was 5.8 GHz with a bandwidth of 10 kHz. Antenna

type input was $\frac{\sin x}{x}$ with vertical polarization and vertical beam width of 4.5 degrees.

Radio signal strength data, often sporadic in nature, was measured at both the transmitter and receiver anytime the backhaul relay link was transmitting data in accordance with testing during the field experiment. Present research uses radio signals measured on 23, 26 and 27 March; and 25, 28 and 29 May. All collections were made between 0800 and 1730 local time.

C. METEOROLOGICAL DATA

Meteorological data included real-time continuous ground meteorological measurements, on-station radiosonde measurements at intervals, and the Navy's Centralized Atmospheric Analysis and Prediction System (CAAPS). All three forms of data were used in the radio propagation effects and effects model predictions.

1. Radiosonde Measurements

The interval radiosonde launches occurred once or twice per day, during the morning and afternoon hours. This occurred to bracket daytime radio data collection rather than to follow the normal 12-hour synoptic interval schedule. Launches took place immediately outside, and beside the TOC at the Mae Ngat dam (LOC: 19 09'45.10N, 99

02'21.00E). Radiosonde launches were not performed on all radio testing days due to equipment failure. Table 4 lists the available radiosonde measurements. The AN/UMQ-12 Mini Rawinsonde System (MRS), a mobile computerized receiver/processor, was used to receive signals from the radiosonde transmitter. RS-80L/RS-80G radiosondes were used for the balloon launches. These units measure the vertical profile of relative humidity, temperature, winds, and pressure at two second intervals. Due to GPS synchronization issues, winds were not measured for either testing period.

Vertical profiles of the in situ Modified refractivity units (M-units), using the AREPS Environment Creator, were calculated with the radiosonde soundings for analysis and required APM input. It is important to note that radio signal strength data were available between the launches and the appropriate data will be addressed later. The radiosonde derived profiles were then used as input to APM to predict propagation loss and received power versus height, for each radio link, using *in situ* meteorology soundings. These APM predictions were compared to *in situ* measured radio signal strength data for consistency and analysis of any statistically significant affect of local refractivity conditions. Results are presented in Chapter IV.

Table 4. On-station radiosonde launches Day/UTC Hour and CAAPS analysis and forecast field DAY/UTC Hour.

Radiosonde	Radiosonde	CAAPS	CAAPS
March	May	March	May
23/01	28/02	23/00	25/00
26/01	28/09	23/01	25/12
26/04	29/01	23/12	28/00
27/00	29/08	26/00	28/02
		26/01	28/09
		26/04	28/12
		26/12	29/00
		27/00	29/01
			29/08
			29/12

2. COAMPS Numerical Weather Model Data

Due to the sparseness of real-time soundings, and for comparison, radiosonde data for upper air refractivity profiles were supplemented with numerical model data from the Fleet Numerical Meteorology and Oceanography Center (FNMOC) in Monterey, California. The Centralized Atmospheric Analysis and Prediction System (CAAPS) is an on-demand, high-resolution, short-term numerical weather prediction system developed for use by military forces in any region of the world (Neu et. al, 2006). CAAPS executes the Navy's Coupled Ocean-Atmosphere Mesoscale Prediction System (COAMPS). Unclassified, NIPRNET CAAPS data was archived for the March and May testing periods at a resolution consisting of four nests: 54/18/6/2km. Typical 24-hr forecast pressure surface, height level, and surface models fields, along with skew-T ASCII profiles, were provided. Table 5 lists the archived gridded binary (GRIB) fields. Previously introduced Table 4 lists CAAPS runs used for analysis, along with radiosonde launch times. CAAPS sounding for TOC-METG relay link LOC: 19.16N, 99.04E. CAAPS sounding for METG-CHCM relay link LOC: 19.13N, 98.94E.

CAAPS field Skew-T soundings, interpolated from grids at 2-km resolution, were compared to available radiosonde soundings for consistency. Vertical profiles of the M-units were created, using the AREPS Environment Creator, for comparison and accuracy with radiosonde *in situ* profiles, and for analysis and required APM input. APM was used to predict propagation loss and received power versus height, for each radio link, using the high-resolution numerical weather model data. Predictions were compared to *in situ* measured radio signal strength data for consistency and analysis of any statistically significant affect of local refractivity conditions forecasted by CAAPS. Results are presented in Chapter IV.

Table 5. Selected CAAPS GRIB Fields. Mesh 1 (54 km) at 6-hr intervals, Mesh 2 (18 km) at 6-hr intervals, Mesh 3 (6 km) at 3-hr intervals, and Mesh 4 (2 km) at 1-hr intervals. (From CAAPS FNMOC Request, 09 May 2007.)

Pressure Surface (1013-850 mb) Air	Height Levels (2-2000 m)	Surface
Air Temperature	Air Temperature	Bucket Total Precipitation
Dew point Depression	Dew Point Depression	Ground/Sea Surface Temperature
Geopotential Height	EM Duct Strength	Ground Wetness
Relative Humidity	EM Duct Thickness	Latent Heat Flux
True U-Velocity Component	EM Duct Top	Planetary Boundary Layer Height
True V-Velocity Component	Relative Humidity	Scale mixing Ratio For Surface
Water Vapor Pressure	True U-Velocity Component	Sea Level Pressure
	True V-Velocity Component	Sea Surface Temperature
	Water Vapor Pressure	Sensible Heat Flux
		Surface Roughness
		Terrain Height

3. Continuous Near-Surface and Ground Measurements

The *in situ* set-up and location of near-surface and surface (ground) measurements appear in Figure 10, are listed in Table 6, and described in the following paragraphs. The data were logged continuously during both testing periods. They were recorded at a one-minute interval using the CR10X Datalogger for Measurement and Control, using a meteorological measurement system built by Naval Postgraduate Faculty. The data logger (<http://www.campbellsci.com/dataloggers>), powered by a solar panel, was enclosed in a weather safe housing next to the measurement station. All measurements were monitored using LoggerNet software support. All temperature probes were calibrated, before deployment, using stirred waterbaths of varying temperatures from 0 to 30°C.



Figure 10. Google Earth Overview of Mae Ngat Dam, Thailand. Note positions of TOC, location site of March ground measurements, and location site of May ground measurements. (Google Earth image, 02 September, 2008.)

Table 6. Near-surface and ground *in situ* meteorological set-up and measuring devices.

Sensor	Manufacturer	Level of Measurement
Pressure	Vaisala PTB101B Barometer (CS105)	Ground Level
Air Humidity & Temperature With radiation shields	Rotronic MP100H & MP400H Humidity and Temperature probes Young Model 41003 multi-plate shield	2, 4, & 8 feet
Vector Wind	R. M. Young Wind Monitor model 05103-L	8 feet
Ground Temperature	Campbell Scientific Apogee Infrared Radiometer (IRR-P)	Positioned at 2 feet and pointed down at soil FOV 22 degree half angle
Soil Temperature	Stelnhart-Hart Temperature Sensor (107-L)	1 Inch under the surface
Soil Moisture	Campbell Scientific Water Content Reflectometer (CS616-L)	2 Inches below the surface

The near-surface measurement station was located approximately 15 m behind the TOC antenna tower during the March testing period and approximately 15 m in front of the TOC antenna tower, in the direct path of the METG tower, during the May testing period. The location of the measurement station was changed during the May testing period for a more precise *in situ* data collection located directly between the first two back haul relay links. The air temperature and relative humidity were measured at three logarithmic levels (2ft, 4ft, 8ft above the surface) with Rotronic Humidity and Temperature Meteorological Probes (MP100H/MP400H) inside a Young Multi-Plate Radiation Shield (Model 41003) (<http://www.youngusa.com>). The probes measure a temperature range from -40 to 60°C with +/- 0.2°C accuracy and a relative humidity range 0 to 100% with +/- 1.5%RH accuracy (<http://www.rotrolic-usa.com/v2/products/meteo/intro.htm#Top>).

Vector wind (speed and direction) was measured with a R.M. Young Wind Monitor (05103-L) using a propeller-type anemometer and a fuselage and tail wind vane. The wind monitor wind speed specifications include a range of 0 to 60 m/s, with an accuracy of +/- 0.3 m/s, a starting threshold of 1.0 m/s, and a gust survival of 100 m/s. The wind direction specifications span from a range of 0 to 360 degrees, with an accuracy of +/- 3 degrees and a starting threshold of 1.1 m/s at 10 degree displacement (<http://www.youngusa.com>).

A Vaisala PTB101B Barometer was used for barometric pressure (CS105). The device measures barometric pressure over a 600 to 1060 mb range, at a temperature range of -40 to 60°C, and with an accuracy of +/- 0.5 mb at +20°C (<http://www.vaisala.com/instruments/products/barometricpressure>).

The surface ground temperature was measured with a Campbell Scientific Apogee Infrared Radiometer (IRR-P) which had a Field of View of a 22-degree half angle (<http://www.campbellsci.com/irr-p>). The soil temperature was measured with a Steinhart-Hart Temperature Sensor (107-L) consisting of a thermistor encapsulated in a cylindrical aluminum housing. The general purpose sensor measures in air, water, and soil with an accuracy of <+/- 0.2°C between 0 and 50°C (<http://www.campbellsci.com/107-l>).

Soil moisture was measured with a Campbell Scientific Water Content Reflectometer (CS616-L) which measures volumetric water content (VWC) from 0% to saturation. The probe consists of two 30 cm long stainless steel rods connected to the measurement electronics which measure the water content using time-domain reflectometry methods. The probe was placed, horizontally, 2 inches below the soil surface. The Reflectometer has an accuracy of +/- 2.5% VWC using standard calibration and within a measurement range of 0 to 50% VWC, a precision of 0.05% VWC, and a resolution of 0.1% VWC (<http://www.campbellsci.com/cs616-l>).

These near-surface and soil measurement data were used to characterize the atmospheric boundary layer during experimentation and to note any diurnal and multi-day trends. A time series of the meteorological measurements including the surface

barometric pressure, wind speed and direction, soil temperature, surface temperature, two-foot air temperature, soil volumetric water content, and calculated specific humidity (calculated using in situ air temperature, relative humidity, and total atmospheric pressure measurements) were captured for further comparison with signal performance data. These results will be presented in Chapter IV.

4. Data Derived from Application of Surface-layer Similarity Theory

In order to increase the resolution of meteorological data available to create refractivity profiles (APM input) for comparison of predicted signal data levels and measured signal data, Monin-Obukhov similarity theory, Garratt (1992), within the atmospheric boundary layer was applied to surface measurements to calculate and extrapolate vertical temperature and specific humidity profiles. These extrapolated profiles were used as input to the AREPS Environment Creator to calculate vertical M-unit profiles for use in APM.

Thirty minute averages of the surface data were calculated for each day during the test periods. Garratt (1992) derives non-dimensional equations with properties independent of external parameters and for which universal profiles can be generated. The relation is described by Garratt (1992) Equation 3.17:

$$k \frac{u}{u_0} = \ln \frac{z}{z_0} \quad (7)$$

where $z/z_0 \gg 1$, and $z_0 \sim 0.1\text{m}$ for general land surfaces.

Substituting specific humidity for u and re-arranging Equation (7), this non-dimensional equation can be used to set-up a height relationship for specific humidity and the ultimate calculation of q^* . The parameter q^* can be equated to the slope, or rate of change, of specific humidity within a constant flux layer:

$$q_1 = \frac{q^*}{k} \ln \frac{z_1}{z_0} \quad (8)$$

$$q_3 = \frac{q^*}{k} \ln \frac{z_3}{z_0} \quad (9)$$

Using the measured values for z_1 , z_3 , q_1 , and q_3 , we can eliminate the dependence on z_0 and estimate q^* with:

$$q^* = k \frac{q_1 - q_3}{\ln \frac{z_1}{z_3}} \quad (10)$$

where q^* is assumed to not change within the constant flux layer, z_1 is the 2-ft measurement height, z_3 is the 8-ft measurement height, and $k = 0.4$ (universal von Karman constant) (Garratt, 1992).

Using the calculated q^* from Equation (10), we can calculate q at an arbitrary height, given a known $q(z)$ within the boundary layer:

$$q_{hgt} - q_x = \frac{q^*}{k} \ln \frac{z_{hgt}}{z_x} \quad (11)$$

Re-arranging Equation (11), we have:

$$q_{hgt} = \frac{q^*}{k} \ln \frac{z_{hgt}}{z_x} + q_x \quad (12)$$

Using a similar physical argument, we can find T at an arbitrary level z_{hgt} with:

$$T_{hgt} = \frac{T^*}{k} \ln \frac{z_{hgt}}{z_x} + T_x \quad (13)$$

Pressure profiles were extrapolated using the hypsometric equation (see, for example, Stull, 2000):

Given a known surface pressure, P_{hgt} can be calculated with:

$$P_{hgt} = P_x \exp\left(\mathbf{g} \frac{z_{hgt} - z_x}{R_d \bar{T}}\right) \quad (14)$$

where pressure (P) is in mb, height (z) in meters, R_d is the gas constant for dry air and $R_d = 287 \text{ J/(kg}\cdot\text{K)}$, \bar{T} is the average temperature in the layer and temperature (T) is in degrees Kelvin, and gravity (g) equals 9.8 m/s^2 .

Refractivity and modified refractivity profiles were created using Eqns (12)-(14) to extrapolate temperature, specific humidity, and pressure profiles. Since Eqns (12)-(14) are based on surface layer scaling, the extrapolations were made up to 100 meters. The calculated M-unit profiles were compared to the lower levels of the radiosonde sounding M-unit profiles for consistency and accuracy of applied theory. The extrapolated profiles served as additional meteorological input in the AREPS Environment Creator, and subsequent M-unit profiles as input for APM. Results are discussed in Section IV.

D. PROPAGATION PREDICTIONS

All Radiosonde profiles, CAAPS numerical weather model analysis and forecast fields, and ground meteorological measurements were considered when obtaining predictions from APM/AREPS for comparison with measured signal strength data. AREPS Environment Creator height versus M-unit profiles served as direct environmental input for APM. Using APM, propagation loss and received power predictions (versus range and height) were calculated using each environmental input for each respective communication suite during the testing period. APM predictions were subsequently compared to measured signal data, at all corresponding time intervals, for accuracy, APM validation, and statistical significance of any identified difference between predictions and measured, as well as the affect of in situ atmospheric refractivity conditions.

E. TERRAIN

A significant environmental impacting feature for surface-to-surface propagation is the change in elevation in the terrain between the sensors. Propagation models can account for this with data on terrain. DTED Level II data terrain was used to conduct this study. DTED Level II terrain data provides terrain elevation with a post spacing of one arc second, or a resolution of approximately 30m. The absolute horizontal accuracy, with

90% Circular Error World Geodetic System (WGS), is ≤ 23 m. The absolute vertical accuracy, with 90% Linear Error Mean Sea Level (MSL), is ≤ 18 m (MIL-PRF-89020B 2000, 23 May 2000). DTED Level II data is the highest resolution of data accepted as input into AREPS. Barrios et al. (2006) describe discrepancies found between DTED and USGS terrain data against actual measured elevation.

The terrain sources used in this analysis did not include foliage or vegetation information as part of the database. Hence, surface properties were not a part of the AREPS prediction, except for overland versus overwater. The actual surface properties of the propagation path varied from dirt to brush to vegetation (Figure 6 and Figure 7). The vegetation was present in the form of patchy trees. The vegetation showed clear seasonal differences between the March and May testing periods.

IV. RESULTS

Real-time meteorological measurements, calculated surface meteorological profiles and CAAPS soundings were environmental input (refractivity profiles) for the application of APM for determining possible atmosphere impact on transmission. Propagation and effects model calculated signal strength were compared to measured signal strength data collected during the testing periods. Signal strength predictions were also obtained using a standard atmosphere and climatology for baseline comparisons.

A. CHARACTERIZATION OF THE IN SITU ENVIRONMENT

1. March Near-surface Time Series

Time series of meteorological surface measurements from March 2007 are shown in Figure 11. Surface pressure clearly exhibited expected semi-diurnal tendency with a maximum and minimum peak. The minimum peak occurred around 2200/2300LT with the maximum peak occurring at approximately 0900/1000LT each day. There was an overall decrease in surface pressure throughout the beginning of the testing period with the minimum surface pressure readings falling on 25 and 26 March and increasing, slightly, thereafter. The pressure trend clearly shows the influence of an evolving large scale synoptic regime for the region.

Winds were fairly consistent throughout the testing period with light and variable winds except for gusty winds from 4-8 m/s picking up by 1200LT and subsiding by 1800LT each day. Winds shifted to westerly, during gusty periods, approaching from the vegetated valley, upslope, towards the face of the dam. The wind direction shifts on 24 and 26 March had associated drops in vapor pressure, indicative of air-mass changes.

The air temperature, ground surface temperature, and soil temperature exhibited a diurnal fluctuation with ground surface temperature fluctuating as much as 20°C. The air temperatures increased, overall, throughout the testing period, based on the maximum for each day. There was an increase (4°C) exhibited from 21 to 27 March, consistent with the steady drop in surface pressure. The variation in ground temperature has possible

significance in this study because it is indicative of how exposed electronic housing temperature could increase in response to radiative heating.

The increase in the soil temperature had a consistent time-lag with the increase in the ground surface temperature. The air temperature consistently lagged both the surface and soil temperatures. The soil temperature maintained an approximate 2°C temperature higher than the air temperature, while the surface temperature maintained an approximate 4-6°C higher temperature. The temperature differences were expected with the ground surface heating up before the air above it.

The air specific humidity increased from 20 to 23 March. The specific humidity dropped approximately 8 (g/kg) on 23 March and steadily increased over the remaining test period. The decrease on 23 March occurred with a large temperature increases. The soil volumetric water content decreased throughout the testing period from which we infer stronger surface latent heat fluxes as the ambient temperature increased.

Radiosonde derived upper air data show a relatively dry atmosphere at the beginning of the testing period. Morning soundings reflect overnight subsidence, and an early morning temperature inversion. The daily maximum surface pressure, minimum surface temperature, and slight moisture variability can be directly attributed to probable nocturnal radiation cooling and overnight fog. Radiation heating of the ground caused temperature inversions to break up by 1200LT each day.

The refractivity and modified refractivity gradient value time series had diurnal fluctuation reaching near-zero values during the evening hours and large negative values during early morning and daylight hours (Figure 12). As a direct result of the daily established temperature inversion immediately above the surface the calculated low-level dM/dz and dN/dz (using surface pressure values, air temperature, saturation vapor pressure, and vapor pressure at height) were mostly negative indicating the presence of a potential shallow ducting layer. However positive refractive gradient ($dN/dz > 0$) values occurred shortly after noon on 23 and 24 March. Larger negative values occurred on the 23 March coinciding with the drop in air specific humidity and lesser drops in volumetric soil water content, sharp rise in air and surface temperature, and the strong low-level

temperature inversion. These near-surface results suggest the lack of super-refractive conditions with respect to impacts on radio propagation, but show possible impacts by subrefraction conditions on 23 and 24 March.

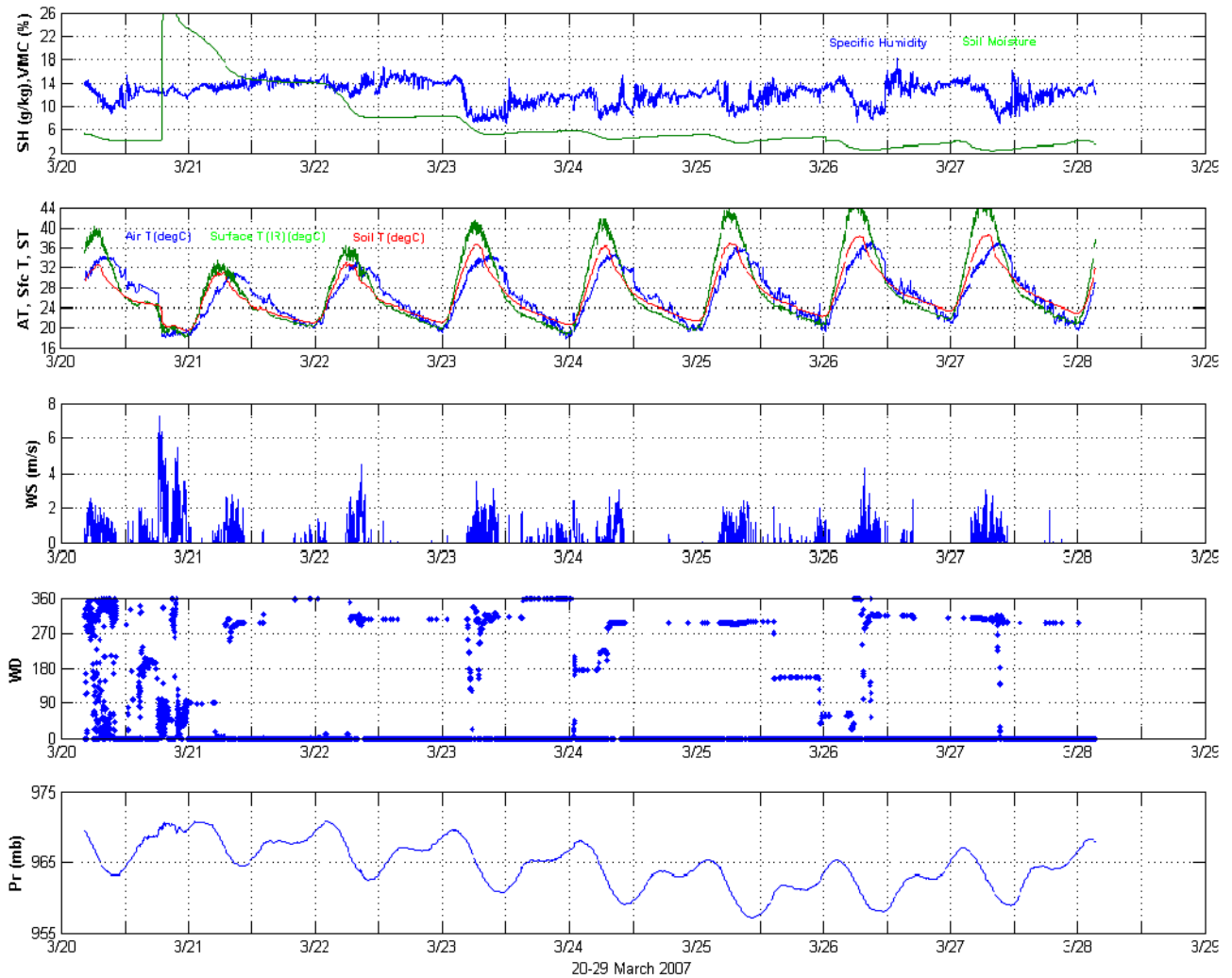


Figure 11. Time series of near-surface meteorological measurements during March test period.

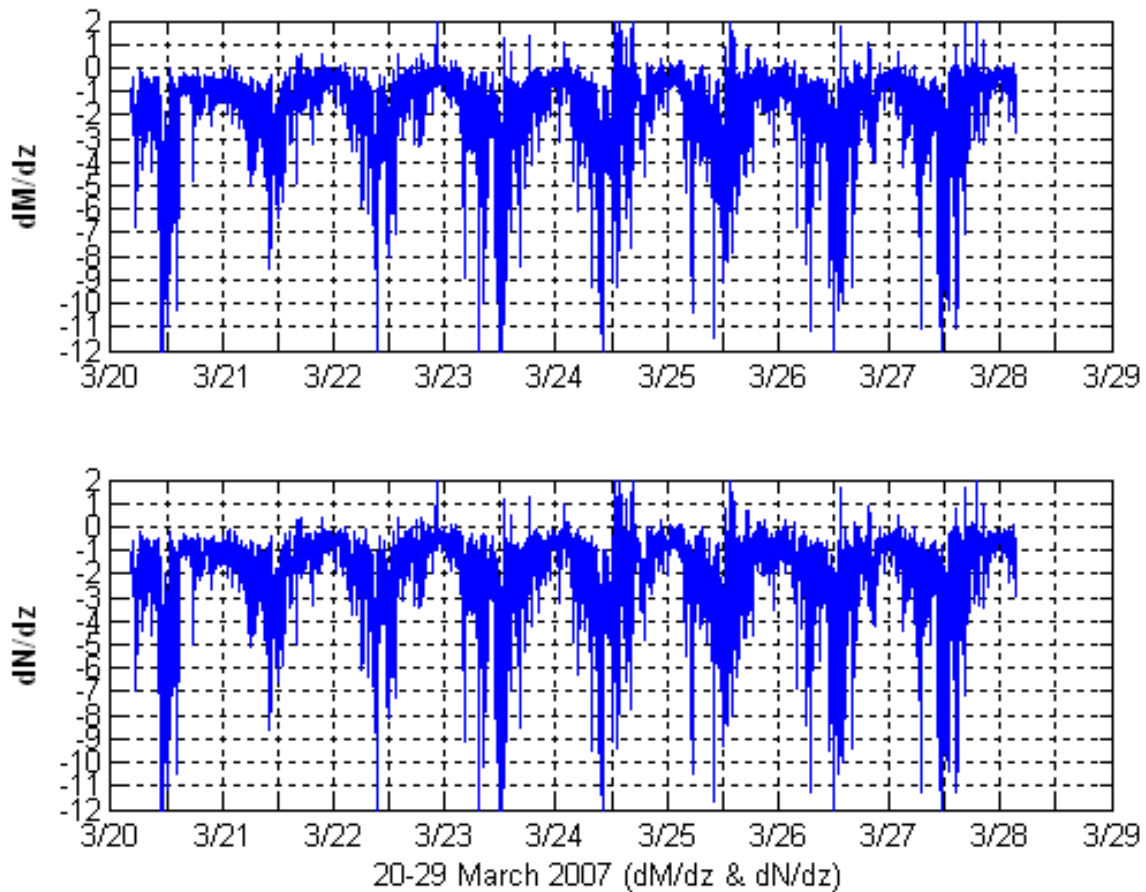


Figure 12. Time series of the change in refractivity index and modified refractivity index with height during the March test period.

2. May Near-surface Time Series

The surface pressure during the May collection campaign also exhibited a semi-diurnal fluctuation; however, the minimum peak occurred an hour later each day and the maximum peaks occurred 1-2 hours earlier (Fig 13). Overall, the surface pressure in May was 4-5mb less than in March. Excluding the diurnal variation, the surface pressure was fairly steady throughout the test period.

Winds were consistent throughout the test period with light and variable winds and daytime increases from 4-8 m/s. The gusty winds seemed to persist for longer

periods than occurred in March and occurred from approximately 0900LT to 2400LT each day. As in March, the gusty winds were generally westerly, tending to easterly in the evening by 1900LT.

The air temperature, ground surface temperature, and soil temperature exhibited a diurnal fluctuation with ground surface temperature fluctuating as much as 25°C. The daily ground temperature maximum increased 8°C throughout the test period. Unlike March variations, very little temperature time-lag existed between the three temperature sources. The soil temperature maintained an approximate 4°C higher than the air temperature. The surface temperature maintained an approximate 12°C higher temperature.

The specific humidity in May, on average, was fairly consistent and about 4 (g/kg) higher than March; while the soil volumetric water content was slightly lower than in March and decreased over the testing period. The time series show greater specific humidity variability during the day hours versus after sunset.

May Radiosonde soundings will be seen to not reflect the same daily subsidence and drying/lifting regime as in March. The monsoonal transition occurs during the months of May and June. The strong high pressure regime weakens and becomes irregular shaped, thus allowing different air masses or variable weather patterns to flow through the region until the SW monsoonal regime sets in bringing continuous warm, moist air. No strong temperature inversions were noted on the morning launches and rapid cooling with height is noted on the afternoon launches. These patterns could be related to the warmer ground surface temperature measured with rapid cooling on the ambient air with height.

May near-surface refractivity and modified refractivity gradient time series also exhibited strong diurnal variability (Figure 14). Note the positive refractivity gradient values as compared to the refractivity gradient values in March.. Both the air temperature and specific humidity were observed as significantly higher than in March. The daily variability increased over the May experimental period. No significant weather features are noted as the cause, on basis of vector wind shifts or pressure tendencies. A

significant aspect of the May time series, unlike in March, is the calculated dM/dz and dN/dz values were mostly positive values, zero, or slightly negative, indicating normal to subrefractive conditions in the lowest levels.

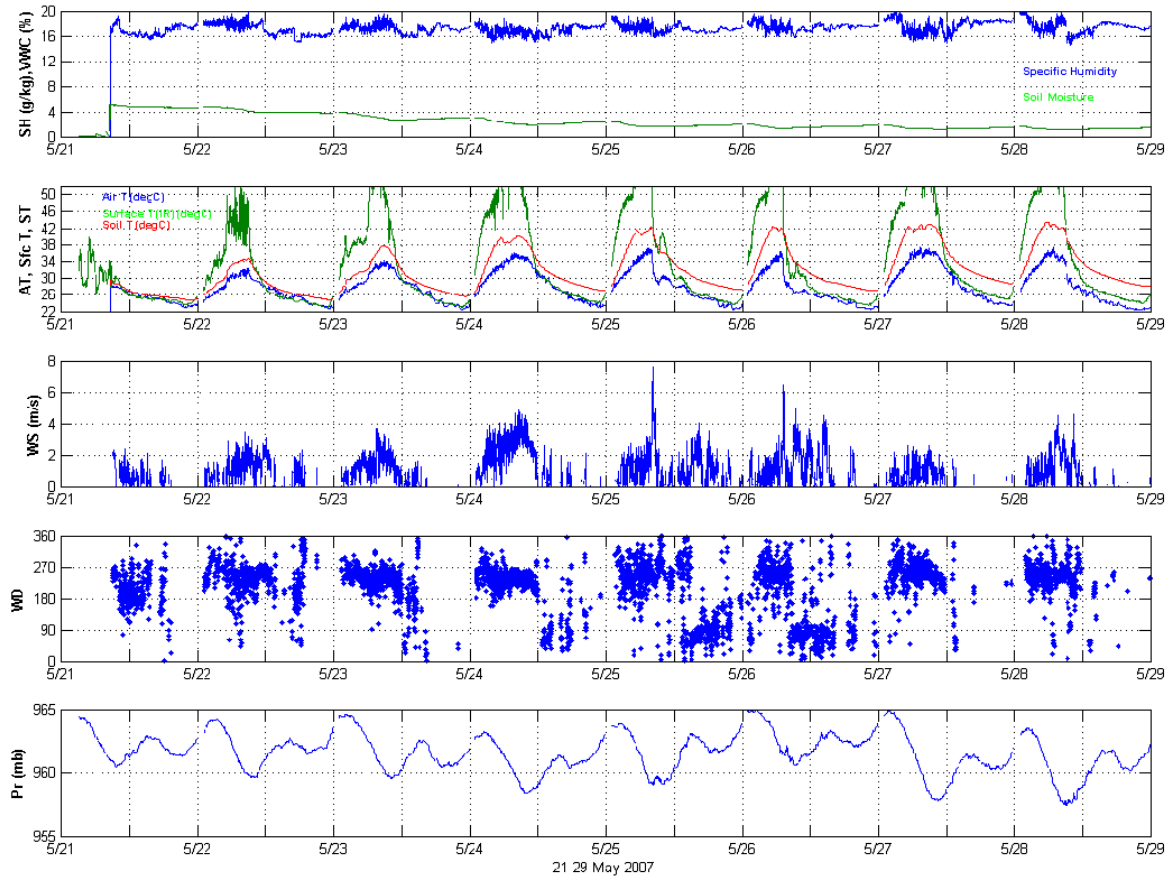


Figure 13. Time series of near-surface meteorological measurements during May test period.

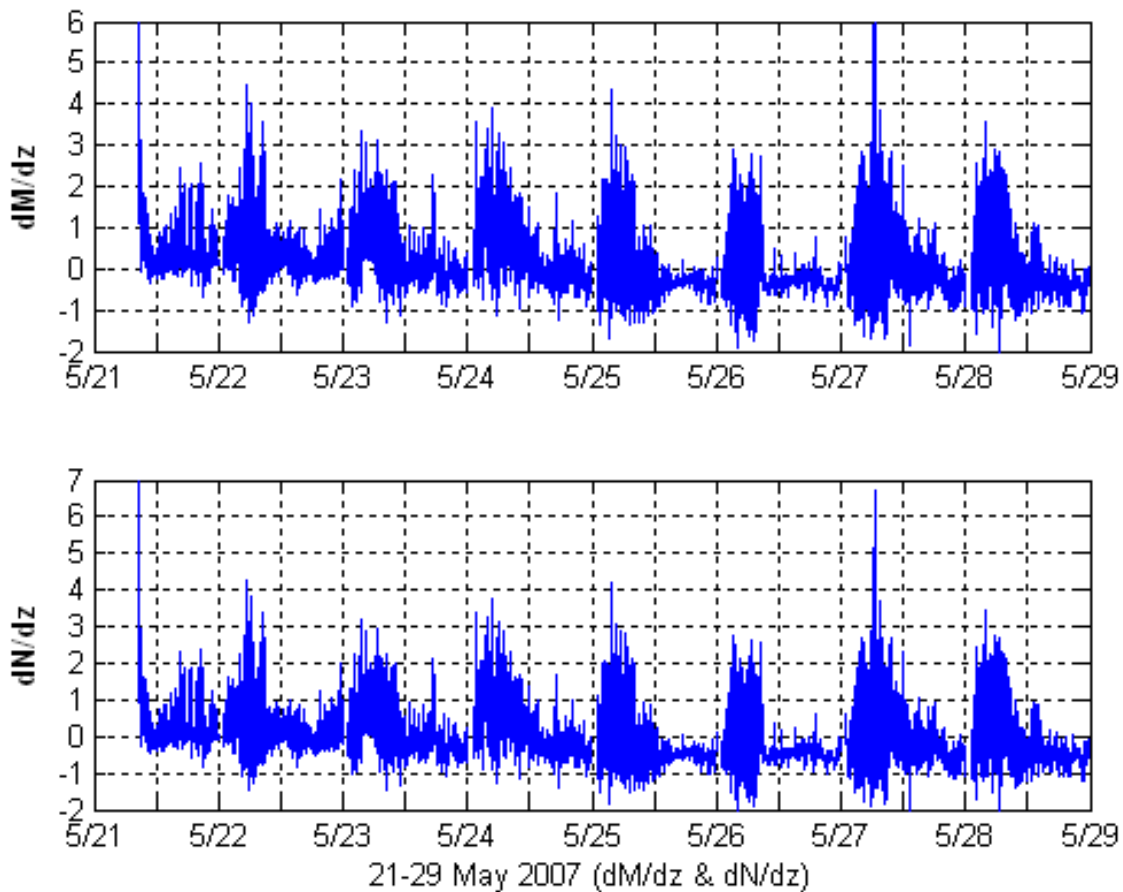


Figure 14. Time series of the change in refractivity index and modified refractivity index with height during the May test period.

B. RADIOSONDE AND CAAPS DERIVED SOUNDINGS

1. March Radiosonde and CAAPS Soundings

The 23 Mar/0000UTC sounding showed a strong, low-level temperature inversion with subsidence aloft. These features are expected during the NE monsoonal regime with its persistent high pressure over the region. The M-profile derived from this launch is shown in Fig 15. An elevated duct existed at a height of approximately 100m (AGL) and is located above the transmitting/receiving antenna. Because the location was well above the surface radio path, the duct should not have an effect on signal transmission. The M-

unit profile reflects the existence of a subrefraction layer at the surface as well as the elevated duct (Figure 15). The CAAPS 23 Mar/0000UTC analysis also showed subsidence and drying aloft and the slight presence of an elevated duct in the M-unit profile. The CAAPS 23 Mar/1200UTC analysis showed low-level drying in the atmosphere and a standard temperature profile.

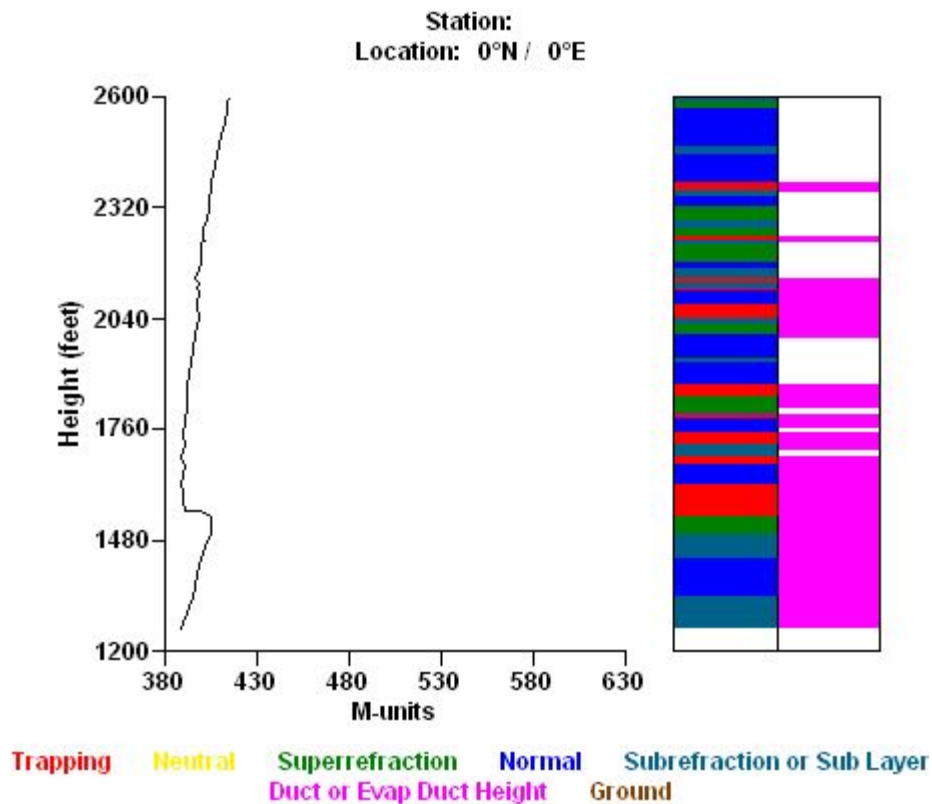


Figure 15. Example M-unit profile from 23 Mar/0100UTC radiosonde launch created using AREPS Environment Creator. Note the low-level subrefraction layer and elevated duct.

The 26 Mar/0100UTC radiosonde profile also showed a strong low-level temperature inversion and rapid drying with height (subsidence). The M-unit profile suggests a trapping layer existed immediately above the surface (Figure 16). The CAAPS 26 Mar/0100UTC forecast also showed a slight low-level temperature inversion with subsidence/drying above. The corresponding CAAPS M-unit profile shows the potential for super-refraction but not a specific trapping layer (Figure 17). AREPS

created M-unit profile graphics in Figure 16 and Figure 17 reflect important, slight differences in the APM inputs based on *in situ* higher vertical resolution radiosonde soundings versus numerical weather model weather data. By the 26 Mar/0400UTC radiosonde launch, temperature and dewpoint temperature profiles were closer to a standard atmosphere. No trapping/ducting surface layers. The CAAPS 26 Mar/1200UTC analysis continued to show rapid drying aloft with a standard temperature profile. The 1200UTC refractivity profile suggested a continued super-refractive layer.

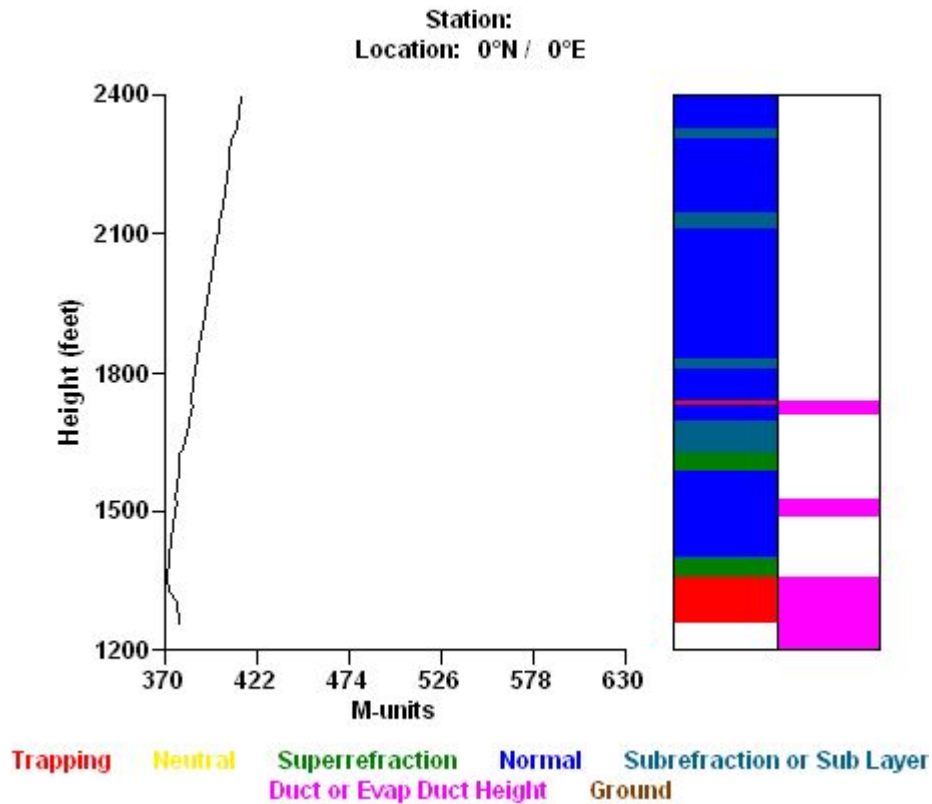


Figure 16. Example M-unit profile from 26 Mar/0100UTC radiosonde launch created using AREPS Environment Creator. Note the low-level trapping.

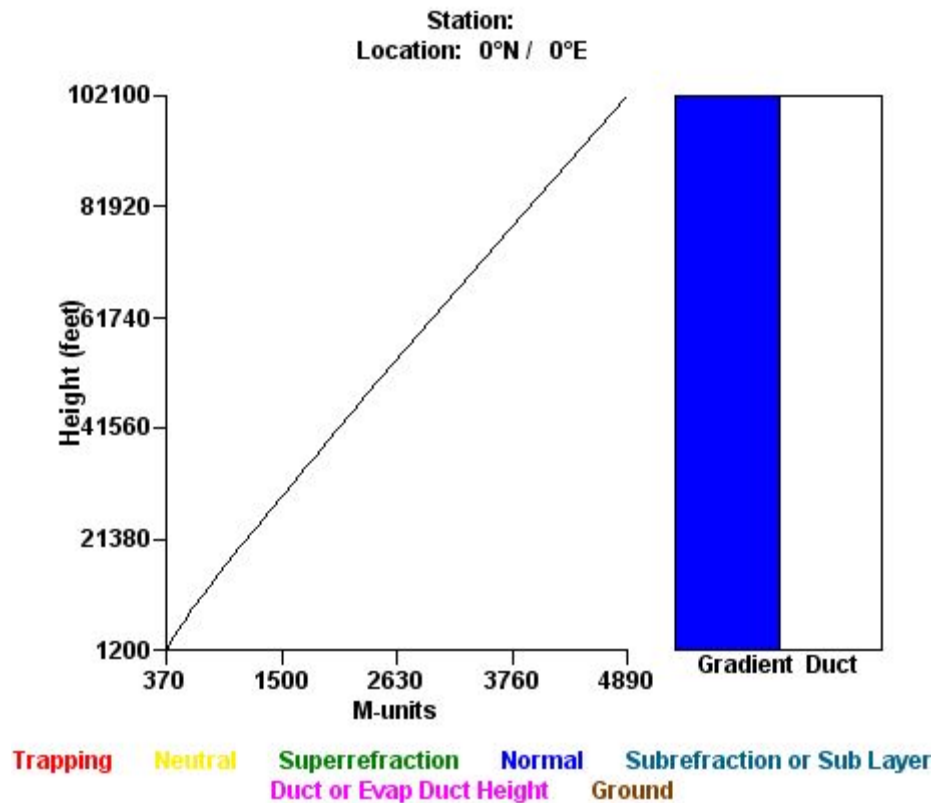


Figure 17. Example M-unit profile from 26 Mar/0100UTC CAAPS analysis created using AREPS Environment Creator. Note the smoothness of the profile and lack of small feature representation.

The 27 Mar/0000UTC radiosonde launch and CAAPS 27 Mar/0000UTC analysis both showed a low-level temperature inversion, and a corresponding decrease in humidity associated with subsidence aloft (Figure 18 and Figure 19). The corresponding radiosonde M-unit profile shows a surface trapping layer and associated-based duct; however, the CAAPS M-unit profile does not (Figure 20 and Figure 21). The features persisted, to a lesser degree, in the 27 Mar/1200UTC CAAPS analysis field, which is not shown. Figure 18 and Figure 19 represent a direct comparison of Radiosonde and CAAPS soundings. Differences between *in situ* soundings and CAAPS analysis field, for the low-level temperature inversion and subsidence aloft, are apparent but they have similar features with lesser gradients. Figure 18 and Figure 19 most importantly show the potential quality and accuracy of the CAAPS analysis fields in a relatively stable environment, as continually seen throughout the field experiment, in this data sparse

environment. Figure 20 and Figure 21 show the respective differences between the M-unit profiles. The differences between the strength of the resultant refractivity gradient structures become quite apparent. The resolutions of the radiosonde sounding better captures the low-level surface features than the CAAPS analysis due to limitation in modeled vertical resolution. These differences will be shown to yield significantly different propagation conditions, i.e., trapping, and no trapping conditions.

The March radiosonde soundings and CAAPS analysis and forecast fields consistently show the presence of a temperature inversion during the morning hours through mid-afternoon. Both also reflect strong subsidence and drying aloft expected during this seasonal time period. The soundings create a potential surface ducting/trapping situation coincident with the temperature inversion and humidity decrease region. The radiosonde shows an associated elevated duct region at the height of the subsidence and drying while CAAPS shows a super-refractive layer. Both non-standard refractivity gradients must be considered, along with the transmission wavelength, when operating in the area.

COASTS 19.16 N 99.04 E 27 MAR 07 0:15 UTC
07032700.txt

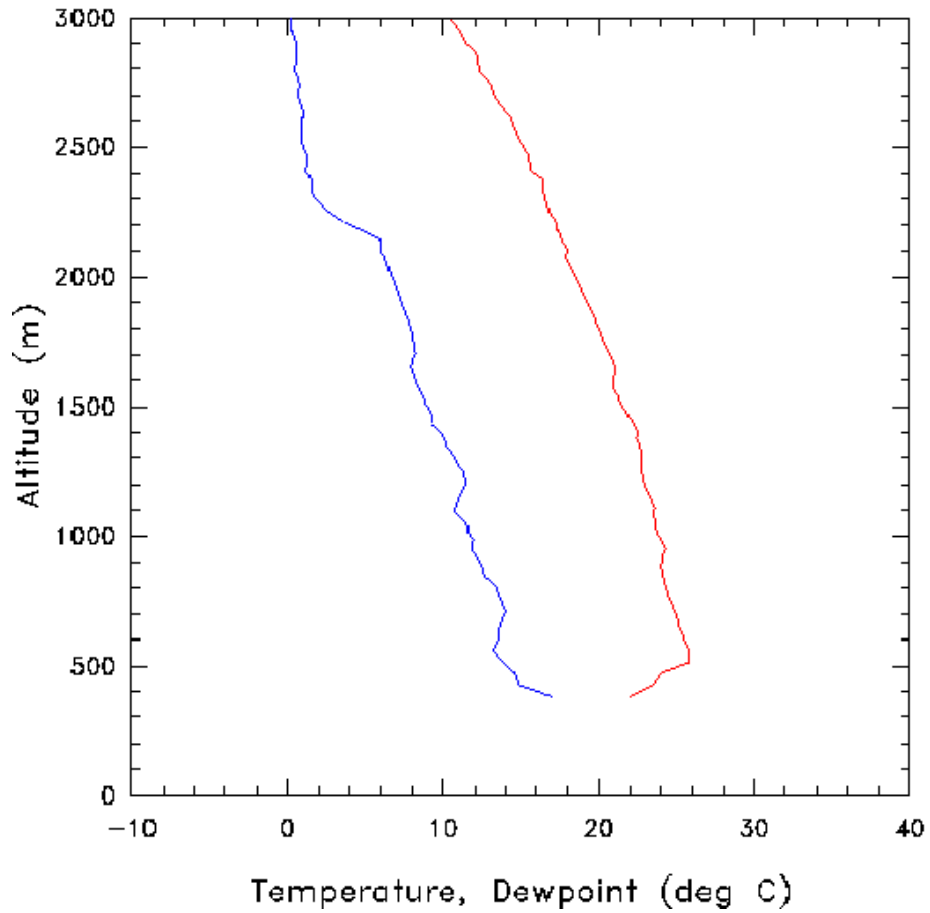


Figure 18. 27 Mar/0000UTC radiosonde launch sounding. The blue line represents the dewpoint temperature and the red line represents the air temperature. Note the low-level temperature inversion and subsidence aloft. Graphic produced using an MS-DOS PLOTSOND program.

COASTS: COAMPS model

03270000.txt

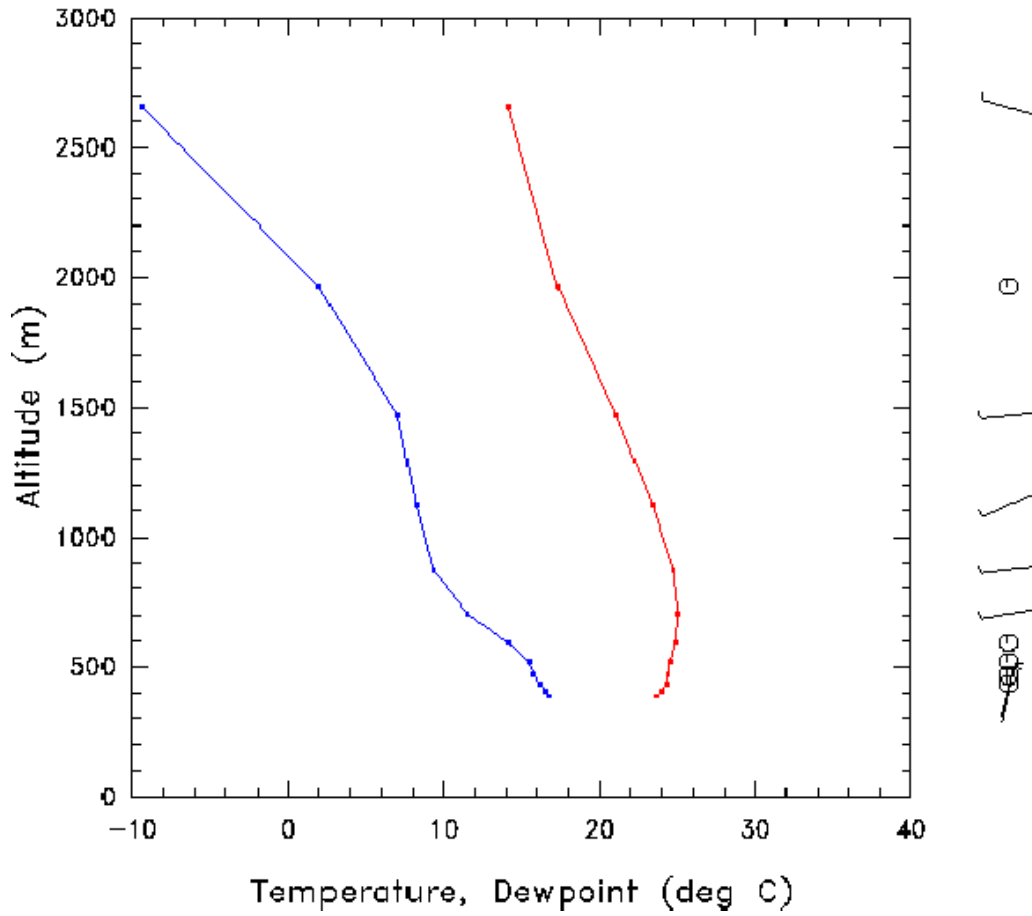


Figure 19. 27 Mar/0000UTC CAAPS analysis field. The blue line represents the dewpoint temperature and the red line represents the air temperature. Note the representative low-level temperature inversion and subsidence aloft. Graphic produced using an MS-DOS PLOTSOND program.

COASTS 19.16 N 99.04 E 27 MAR 07 0:15 UTC
07032700.txt

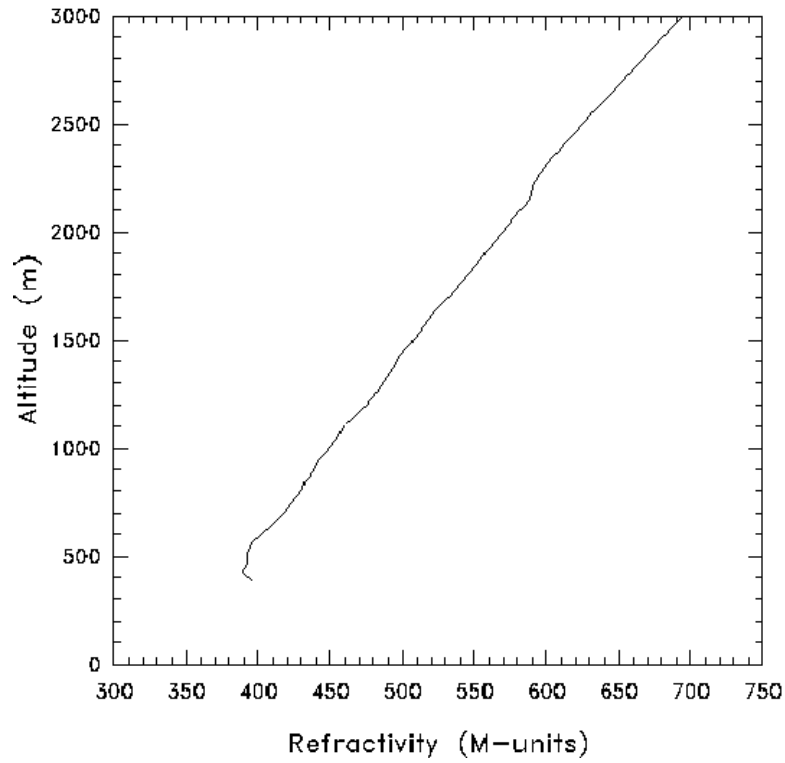


Figure 20. 27 Mar/0000UTC radiosonde Modified refractivity profile. Note the low-level surface duct. Graphic produced using an MS-DOS PLOTSOND program.

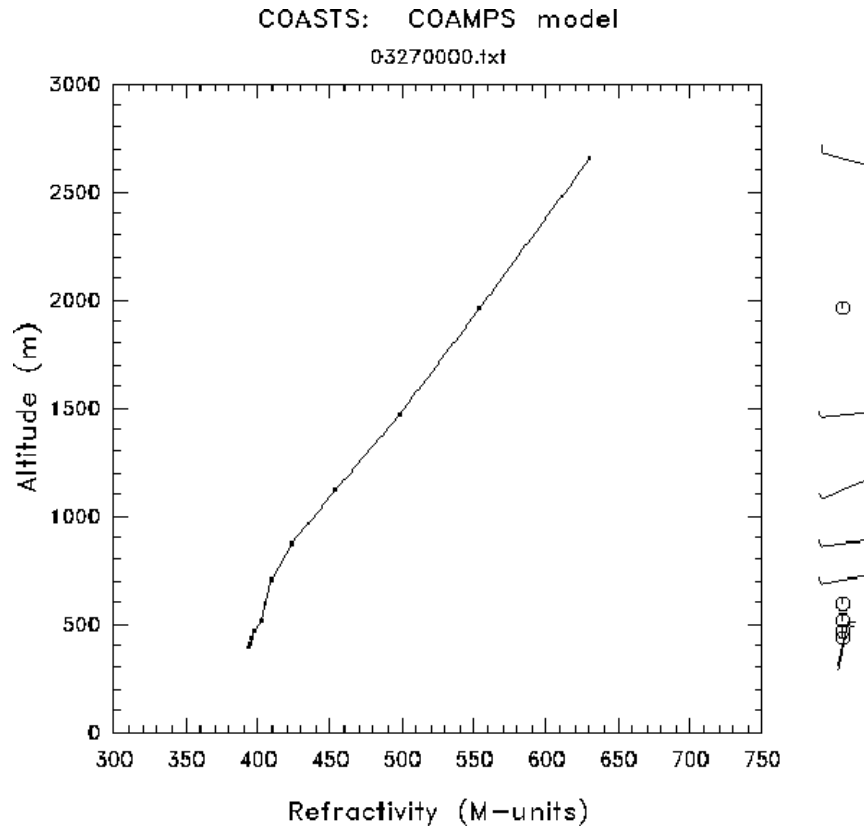


Figure 21. 27 Mar/0000UTC CAAPS analysis field Modified refractivity profile. Note the slight representation of a low-level surface duct. Graphic produced using an MS-DOS PLOTSOND program.

2. May Radiosonde and CAAPS Soundings

Radiosonde information is not available for 25 May due to equipment malfunction. May radiosonde and CAAPS soundings are not included in this write-up. The 25 May/0000UTC CAAPS analysis field had a relatively strong, shallow temperature inversion at the surface with drying aloft. The M-unit derived profile reflected a shallow surface-based duct. The refractivity profile extends the ducting layer to approximately 100m in depth. By the 25 May/1200UTC CAAPS run, analysis fields show refractivity profiles that reflect standard refractivity gradients.

The 28 May/0200UTC sounding and CAAPS forecast fields showed subsidence and drying aloft. The respective AREPS derived M-unit profiles suggest super-refractive propagation in this region. An elevated trapping layer was coincident with the subsidence aloft in both M-unit profiles; however, because of its location, it should not

affect signal transmission. The 28 May/0900UTC radiosonde launch showed rapid cooling and drying above the surface (not reflected in the CAAPS 28 May/1200UTC analysis field) and the derived M-unit profile reflects a strong surface-based duct.

The 29 May/0100UTC radiosonde launch showed decreasing temperature and slight moistening with height. The derived M-unit profile suggests surface trapping. The CAAPS 29 May/0000UTC analysis field does not fully represent and capture the surface conditions measured by the radiosonde. However, the field does show a shallow temperature inversion and drying, with cooling and moistening above. The resultant M-unit profile does not reflect a definable trapping/ducting layer. A shallow, but not pronounced, temperature inversion existed at the 29 May/0800UTC radiosonde launch. The resultant M-unit profile is fairly standard with a slight, potential subrefractive layer above the surface. The CAAPS 29 May/1200UTC analysis field does not capture the temperature inversion or non-standard refractivity.

The months of May and June, climatologically the monsoonal transition season, result in varying refractivity conditions dependent on the changing *in situ* environment. The three days of measurements reflect the changing upper air profiles from a non-standard to a fairly standard atmosphere and from non-standard to standard refractivity gradients, respectively. During the transition season, *in situ* measurements or accurate numerical model input become important for environmental and atmospheric analysis to capture the fluctuating environment and refractivity response. Operators must be aware of the fluctuating environment and potential consequences for signal transmission.

C. RESULTS OF CORRELATION OF METEOROLOGICAL, GROUND MEASUREMENTS AND MEASURED SIGNAL STRENGTH

A statistical correlation was computed between the measured signal received power and the *in situ* ground temperature, air temperature (4 ft), relative humidity (4 ft), soil temperature, calculated specific humidity, calculated saturation vapor pressure, and calculated vapor pressure, Tables 7 and 8. March data yields stronger correlation coefficients with received power; however, the sign of the correlation is not consistent from day to day. For example, on 23 and 27 March, air temperature had a negative

correlation of 0.86 with RSSI and relative humidity had a positive correlation of 0.89 and 0.86 to RSSI, respectively. On 26 March, air temperature showed a positive correlation of 0.85 to RSSI and relative humidity showed a negative correlation of 0.93 to RSSI (Table 7). On 23 and 27 March, ground temperature had a negative correlation of 0.82 and 0.53 to RSSI, respectively. On 26 March, ground temperature showed a positive correlation of 0.93 to RSSI. Similar results were found with all the atmospheric variables in March. Calculations were redone to ensure statistical accuracy of the observed variables. The resultant correlation fluxes show that a direct relationship cannot be drawn between specific atmospheric variables and signal strength using this data.

Correlation values during the May testing period do not reflect as dramatic a difference between day to day values, or as strong a correlation between the atmospheric variables and measured received signal strength as observed in March. Generally, May data yielded weak correlation values of 0.5 or less (Table 8). The small, daily variation of the actual individual atmospheric variables, coupled with relatively flat signal data, helps to explain the weak correlation values. Table 9 and Table 10 show the mean, standard deviation, minimum measurement recorded, and maximum measurement recorded for the signal strength data, the 4-ft air temperature, the 4-ft relative humidity, and the calculated specific humidity for each day of testing. Little variability occurs in May's signal strength data. The mean RSSI varied between -82 and -83 dB with a 0.2 to 0.4 standard deviation, as compared to March's RSSI which varied between -77 to -89 dB with a up to a 3.4 standard deviation. May's atmospheric variables similarly showed a quantifiable smaller daily fluctuation between maximum and minimum values.

Figure 12 and Figure 14 show that refractivity conditions varied between the March and May test periods. These near-surface results during March suggest the lack of super-refractive conditions with respect to impacts on radio propagation, but show possible impacts by subrefraction conditions on 23 and 24 March. May's calculated dM/dz and dN/dz values were mostly positive values, zero, or slightly negative, indicating normal to subrefractive conditions in the lowest levels. The potential of subrefractive conditions is expected as the ground temperature rises and surface heating increases. The correlation between dM/dz and dN/dz and received power was conducted to show if there

is a direct relationship between subrefractive conditions and resultant signal strength (Table 11). The resultant correlation fluxes show that a direct relationship cannot be drawn between subrefraction and signal strength using this data.

Another possible environmental impact on signal strength can result from the direct heating of the communication equipment. Unfortunately, incoming solar radiation, circuit board temperatures, and equipment temperatures were not measured during the field experiment. The communication suite vendors chose not to compromise the water-tight integrity of the wireless access points, by inserting a requested thermometer, prior to field deployment. The measured surface heating can serve as an analog to the increased, direct heating of the wireless access points. Increased circuit board and equipment temperatures both increase the electronic resistance of the equipment and, therefore can adversely affect and degrade the signal strength overtime.

Table 7. Correlation table of various atmospheric variables to the measured Received Signal Strength Indicator (received power) during the March testing period.

	23 March	26 March	27 March
T ground to RSSI	-0.820	0.935	-0.530
T air to RSSI	-0.869	0.853	-0.867
RH to RSSI	0.893	-0.934	0.863
T soil to RSSI	-0.800	0.889	-0.576
SH to RSSI	0.563	-0.909	0.766
Vap. Press to RSSI	0.570	-0.907	0.769

Table 8. Correlation table of various atmospheric variables to the measured Received Signal Strength Indicator (received power) during the May testing period.

	25 May	28 May	29 May
T ground to RSSI	-0.588	-0.098	-0.577
T air to RSSI	-0.573	-0.130	-0.628
RH to RSSI	0.570	0.125	0.377
T soil to RSSI	-0.632	0.324	-0.497
SH to RSSI	0.450	0.032	-0.755
Vap. Press to RSSI	0.454	0.037	-0.806

Table 9. March received power, air temperature, relative humidity, and specific humidity statistics.

23 Mar				
	Received Power	Temperature	Relative Humidity	Specific Humidity
Mean	-81.825	28.296	63.076	0.014
Std Dev	1.195	2.027	11.240	0.001
Min	-83.354	21.000	48.700	0.013
Max	-77.934	29.100	92.300	0.018
26 Mar				
	Received Power	Temperature	Relative Humidity	Specific Humidity
Mean	-82.690	32.550	35.750	0.011
Std Dev	3.432	3.209	14.798	0.002
Min	-89.190	27.700	21.100	0.009
Max	-80.565	36.100	59.800	0.015
27 Mar				
	Received Power	Temperature	Relative Humidity	Specific Humidity
Mean	-83.136	31.496	44.241	0.013
Std Dev	0.908	4.627	18.024	0.002
Min	-85.107	19.800	18.900	0.008
Max	-80.729	37.600	88.500	0.018

Table 10. May received power, air temperature, relative humidity, and specific humidity statistics.

25 May				
	Received Power	Temperature	Relative Humidity	Specific Humidity
Mean	-82.996	29.976	60.180	0.016
Std Dev	0.225	1.250	6.640	0.001
Min	-83.570	27.800	50.800	0.015
Max	-82.420	31.900	73.500	0.018
28 May				
	Received Power	Temperature	Relative Humidity	Specific Humidity
Mean	-83.015	34.446	46.436	0.016
Std Dev	0.486	1.185	3.599	0.001
Min	-83.945	31.600	40.700	0.015
Max	-81.551	36.600	55.900	0.018
29 May				
	Received Power	Temperature	Relative Humidity	Specific Humidity
Mean	-83.801	26.733	86.527	0.020
Std Dev	0.263	0.258	0.944	0.0001
Min	-84.120	26.400	84.700	0.020
Max	-83.293	27.200	87.500	0.020

Table 11. Correlation table of dN/dz and dM/dz to the measured Received Signal Strength Indicator (received power) during the March and May testing periods.

	23 March	26 March	27 March
dN/dz & dM/dz	0.344	0.852	-0.322
	25 May	28 May	29 May
dN/dz & dM/dz	0.069	-0.039	0.049

D. RESULTS WITH EXTRAPOLATED TEMPERATURE, SPECIFIC HUMIDITY, AND MODIFIED REFRACTIVITY PROFILES

The extrapolated temperature, specific humidity, and M-unit profiles are used to describe refraction gradients in the lowest level of the boundary layer where radiosonde soundings and numerical weather model vertical resolution cannot fully capture the granularity of small features and potential non-standard refractivity gradient structure(s). Figure 22 shows an example of the extrapolated temperature, specific humidity, and resultant modified refractivity profiles based on logarithmic surface measurements. All extrapolated profiles were compared to the radiosonde and respective CAAPS analysis or forecast soundings for validation of methodology. The resultant modified refractivity slope (from the extrapolated temperature and specific humidity profiles) matched the slope of both the radiosonde and CAAPS derived M-unit profiles (Figure 23). Minor differences in initial temperatures and specific humidity create M-unit profiles that lie at different calculated refractivity values when directly compared; however, the slope and variations of the actual gradient of the profiles captures the trend correctly and is most important to assessing ducting and trapping layers.

The fixed collection procedures used within this research is not suitable for sole use within a predictive tool such as APM, which require profiles. The height of the surface measurements (2ft, 4ft, 8ft) used to create the profiles were too low to capture variability in the atmosphere above the surface layer (in this case, the bottom 10% of the

boundary layer). Figure 24 shows an important *in situ* increase in specific humidity with height as measured with the radiosonde sounding. Figure 25 shows an increase in the *in situ* air temperature with height (temperature inversion) present that the logarithmic ground measurements and extrapolations did not represent. The ground measurements sense the initial heating of the ground at sunrise with the cooler air layer adjacent. The lowest level of changes in temperature and specific humidity with height will change the gradient and structure of refractivity profiles, but not necessarily accurately represent the mid and upper boundary layer. Any repeat of the described methodology should use a height measurement well above the bottom three measurements to capture vertical changes in the atmosphere and adjust the extrapolation accordingly.

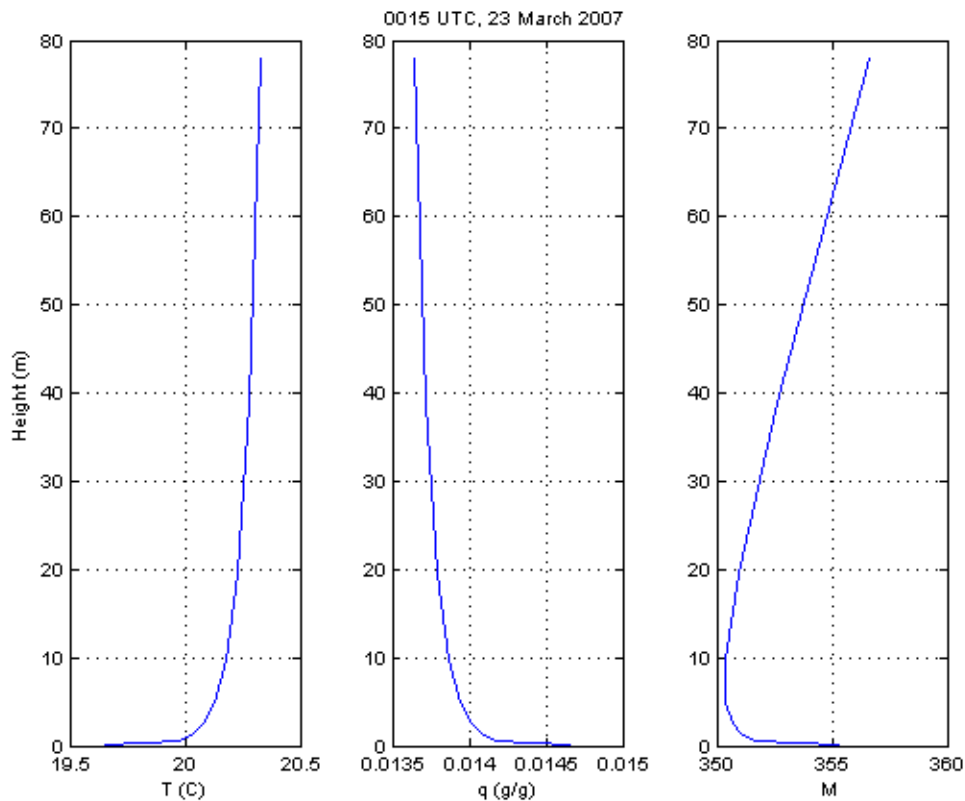


Figure 22. Example of an extrapolated temperature, specific humidity, and M-unit profiles used for analysis. Extrapolation profiles were calculated from averaged 30 minute surface meteorological data on the 23 March from 0000UTC to 0030UTC.

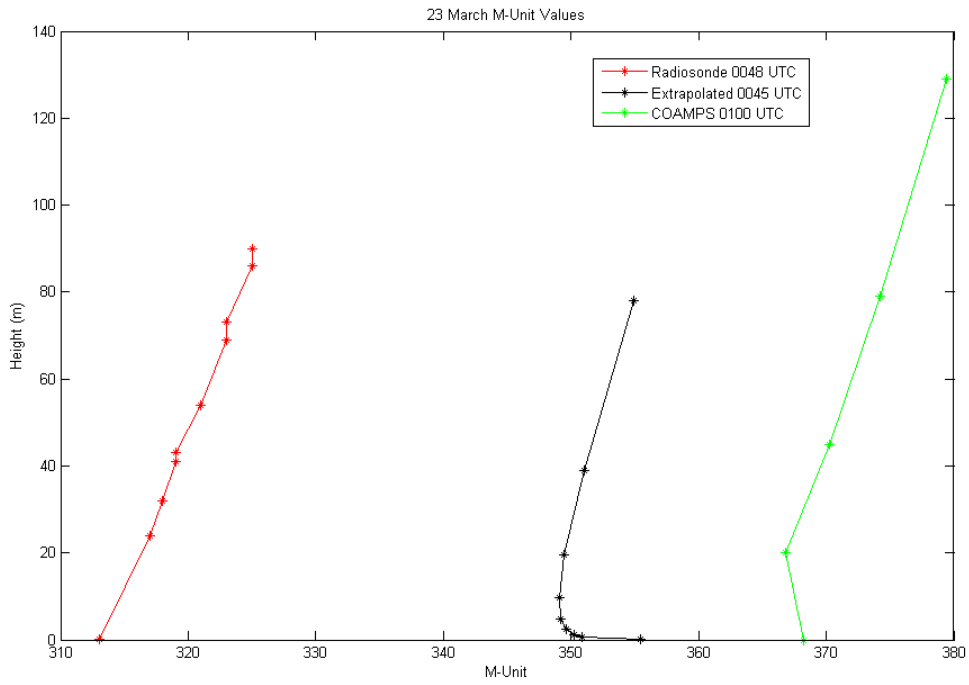


Figure 23. Comparison of M-unit profiles derived from 23 Mar/0100UTC radiosonde launch, CAAPS 23 Mar/0100UTC analysis fields, and 30 min averaged surface meteorological data on 23 March from 0030UTC to 0100UTC.

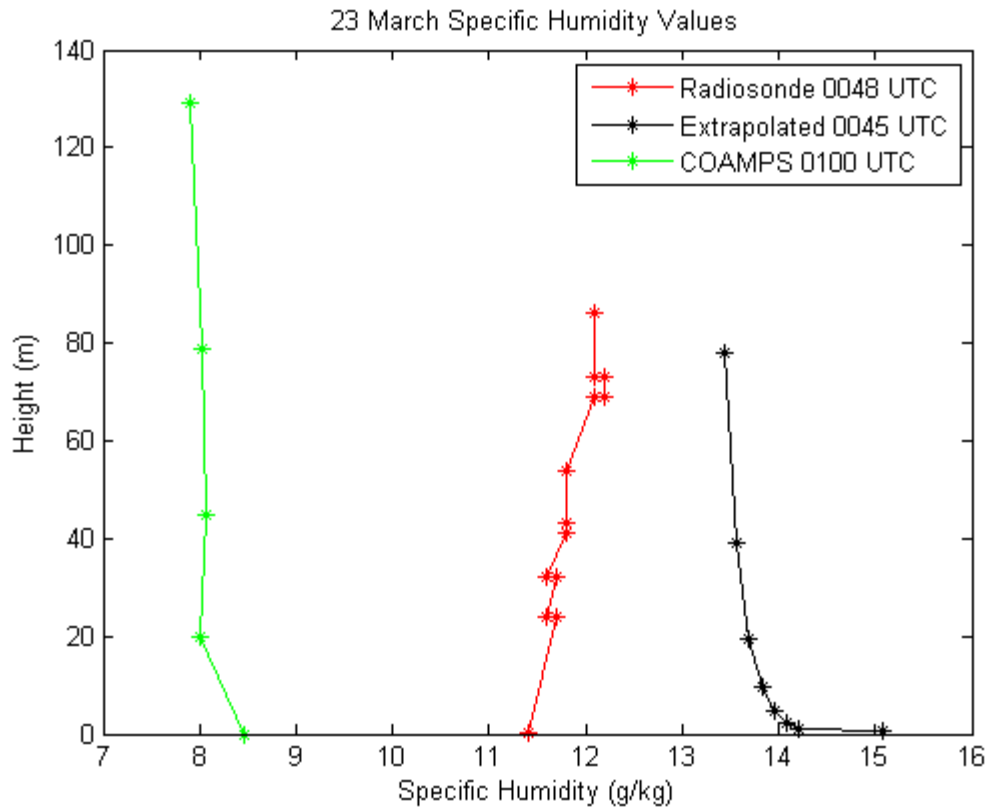


Figure 24. Comparison of specific humidity profiles derived from 23 Mar/0100UTC radiosonde launch, CAAPS 23 Mar/0100UTC analysis fields, and 30 min averaged surface meteorological data on 23 March from 0030UTC to 0100UTC.

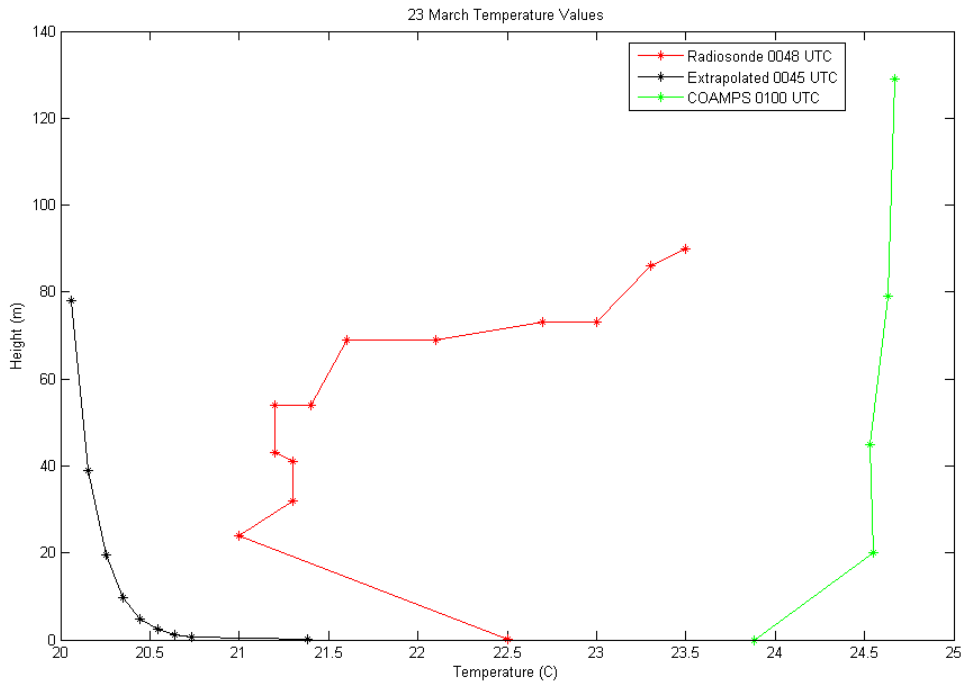


Figure 25. Comparison of temperature profiles derived from 23 Mar/0100UTC radiosonde launch, CAAPS 23 Mar/0100UTC analysis fields, and 30 min averaged surface meteorological data on 23 March from 0030UTC to 0100UTC.

E. OBSERVED VERSUS OBSERVED SIGNAL DATA

Application of APM did not adequately track or quantitatively predict the observed signal. APM error was approximately 9 dBm in March and 12 dBm in May (Table 12 and Table 13). Barrios et al. (2006) found similar results. For each case, the predicted received power was less than the observed. During the May test period, APM under-predicted propagation loss by 10-15 dB (Table 14). Link loss data from March is not available. Operator set-up of the communications system, within AREPS, and AREPS limitations must be considered when evaluating the model validation and results.

The new communications impact prediction system built using the AREPS Communications editor was derived from, and in accordance with, Redline and Motorola communications suite specifications information. Figure 26 shows the input fields within the AREPS communications editor.

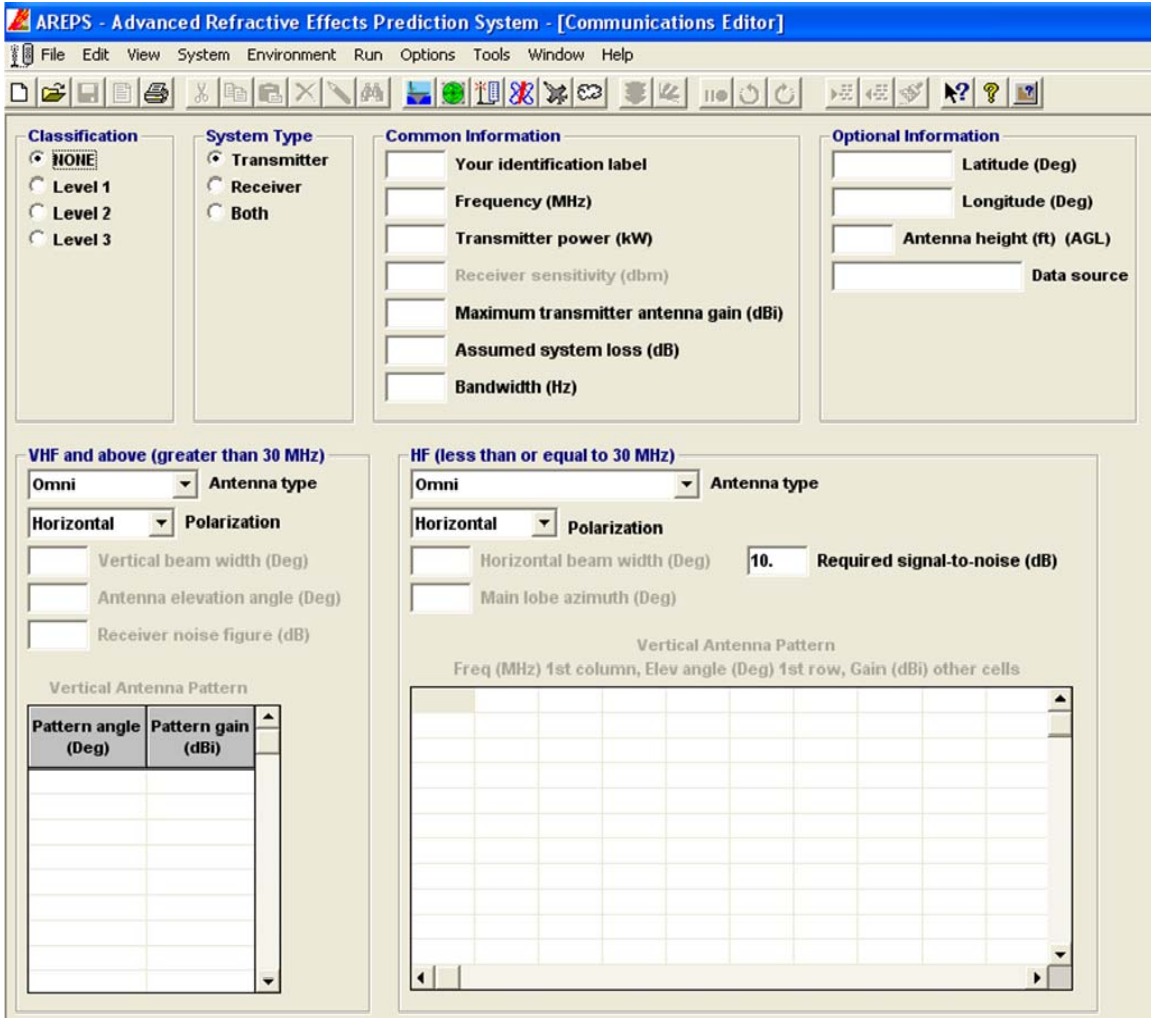


Figure 26. AREPS Communication Editor for building a new communications system within the TDA.

Table 12. Mean and standard deviation of APM predicted received power (RSSI) and measured signal received power for TOC-METG radio link. March measured RSSI not available.

Date: 25 May						
	Radioonde	CAAPS	Extrapolated	Std Atm	Clmo	Measured
Mean	N/A	-88.23	-87.87	-87.89	-88.27	-80.25
Std Dev	N/A	0.223	0.105	N/A	N/A	0.387
Date: 28 May						
	Radioonde	CAAPS	Extrapolated	Std Atm	Clmo	Measured
Mean	-86.41	-88.14	-87.83	-87.89	-88.27	-79.74
Std Dev	1.287	0.474	0.161	N/A	N/A	0.610
Date: 29 May						
	Radioonde	CAAPS	Extrapolated	Std Atm	Clmo	Measured
Mean	-89.19	-88.05	-87.98	-87.89	-88.27	-79.48
Std Dev	1.365	N/A	N/A	N/A	N/A	0.263

Table 13. Mean and standard deviation of APM predicted received power (RSSI) and measured signal received power for METG-CHCM radio link.

Date: 23 March						
	Radioonde	CAAPS	Extrapolated	Std Atm	Clmo	Measured
Mean	-95.77	-94.05	-94.44	-95.18	-94.88	-81.83
Std Dev	N/A	0.199	0.260	N/A	N/A	1.158
Date: 26 March						
	Radioonde	CAAPS	Extrapolated	Std Atm	Clmo	Measured
Mean	-94.35	-94.16	-93.96	-95.18	-94.88	-82.69
Std Dev	0.198	0.206	0.258	N/A	N/A	3.432
Date: 27 March						
	Radioonde	CAAPS	Extrapolated	Std Atm	Clmo	Measured
Mean	-104.32	-94.18	-94.27	-95.18	-94.88	-83.14
Std Dev	N/A	0.225	0.322	N/A	N/A	0.908
Date: 25 May						
	Radioonde	CAAPS	Extrapolated	Std Atm	Clmo	Measured
Mean	N/A	-94.56	-95.59	-95.21	-95.26	-82.99
Std Dev	N/A	0.021	0.243	N/A	N/A	0.225
Date: 28 May						
	Radioonde	CAAPS	Extrapolated	Std Atm	Clmo	Measured
Mean	-94.04	-94.35	-95.05	-95.21	-95.26	-83.02
Std Dev	N/A	0.250	0.622	N/A	N/A	0.486
Date: 29 May						
	Radioonde	CAAPS	Extrapolated	Std Atm	Clmo	Measured
Mean	-94.90	-94.68	-94.80	-95.21	-95.26	-83.80
Std Dev	N/A	N/A	N/A	N/A	N/A	0.263

Table 14. Mean and standard deviation of APM predicted propagation loss and measured signal link loss for TOC-METG radio link.

Date: 27 March						
	Radioonde	CAAPS	Extrapolated	Std Atm	Clmo	Measured
Mean	132.10	133.99	133.93	134.40	133.9	148.9
Std Dev	N/A	0.951	0.104	N/A	N/A	6.819
Date: 25 May						
	Radioonde	CAAPS	Extrapolated	Std Atm	Clmo	Measured
Mean	N/A	134.43	133.99	134.10	134.40	148.25
Std Dev	N/A	0.275	0.145	N/A	N/A	0.361
Date: 28 May						
	Radioonde	CAAPS	Extrapolated	Std Atm	Clmo	Measured
Mean	132.40	134.40	133.97	134.10	134.40	147.72
Std Dev	1.131	0.374	0.140	N/A	N/A	0.671
Date: 29 May						
	Radioonde	CAAPS	Extrapolated	Std Atm	Clmo	Measured
Mean	135.35	134.20	134.20	134.10	134.40	147.47
Std Dev	1.202	N/A	N/A	N/A	N/A	0.432

Antenna gain was assumed at 28 dBi or the max antenna gain of the respective equipment (specifications: 23-28 dBi). Antenna type was selected as $\frac{\sin x}{x}$, to most closely resemble signal wave form, and antenna elevation angle was assumed zero based on conversation with network administrator. An incorrect antenna angle could alone cause significant prediction error of signal transmission received. Bandwidth was entered as 10 MHz, or the max allowable within AREPS. The actual bandwidth, during testing, was 30 MHz. Receiver noise figure was assumed zero and receiver sensitivity was assumed at the max specifications, or -91 dBm. No *in situ* measurements were made for the actual receiver sensitivity and no receiver noise figure calculations were completed. Assumed system loss was 0.365 dB for the Motorola equipment and 6 dB for the Redline equipment in accordance with link budget worksheets. The DTED II terrain was not verified, on-station, for accuracy and may not fully account for the varied terrain and vegetation growth affects. Finally, system set-up did not allow explicit specification of the digital OFDM signal type. This sole factor, alone, would cause over-prediction of loss of received power.

A significant outcome of this research is with respect to the meteorological data input and the APM output. Figures 27 through 31 show the various environment refractivity input for each type of meteorological data set from the 23 March. The extrapolated M-unit profile has the greatest resolution at lower-levels, followed by the radiosonde sounding, then the CAAPS analysis, then climatology, and finally the standard atmosphere. Table 15 lists the M-unit entries and vertical resolution of each atmospheric input. There is a large variation found between the five atmospheric input vertical resolutions and derived refractivity profiles; however, there is a small, almost negligible variation in the APM predicted received power and link loss (Table 12, Table 13, and Table 14). All predictions are within one dBm for the received power and one dB for the signal propagation link loss. The error between the predicted and the observed signal remained the same for each data input.

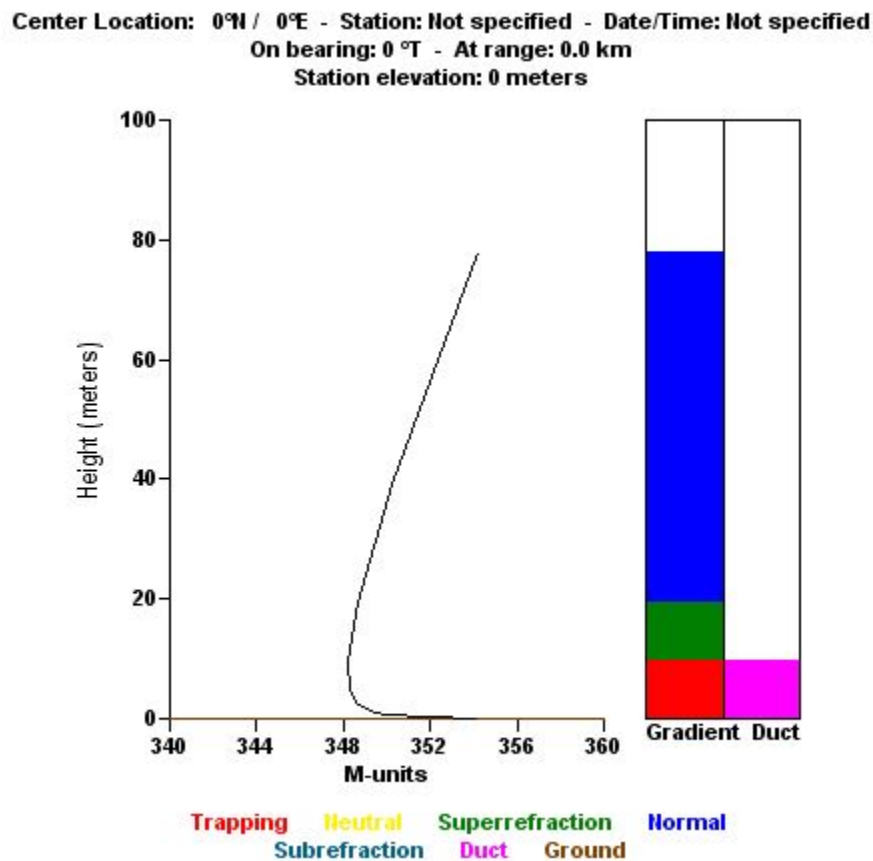


Figure 27. Extrapolated 23 Mar/0115UTC AREPS M-unit graphic.

Center Location: 0°N / 0°E - Station: Not specified - Date/Time: Not specified
On bearing: 0°T - At range: 0.0 km
Station elevation: 383 meters

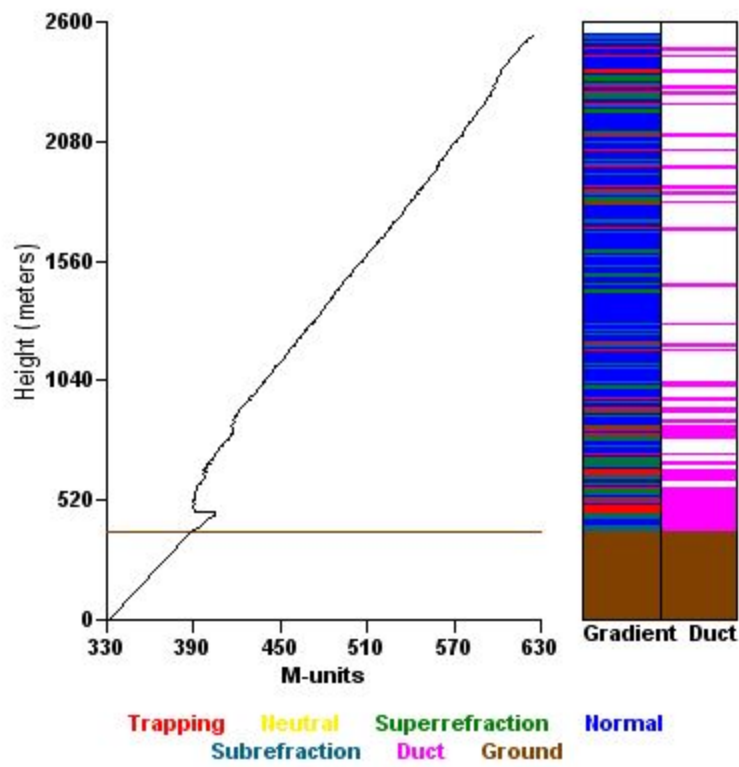


Figure 28. Radiosonde sounding 23 Mar/0100UTC AREPS M-unit graphic.

Center Location: 0°N / 0°E - Station: Not specified - Date/Time: Not specified
On bearing: 0°T - At range: 0.0 km
Station elevation: 0 meters

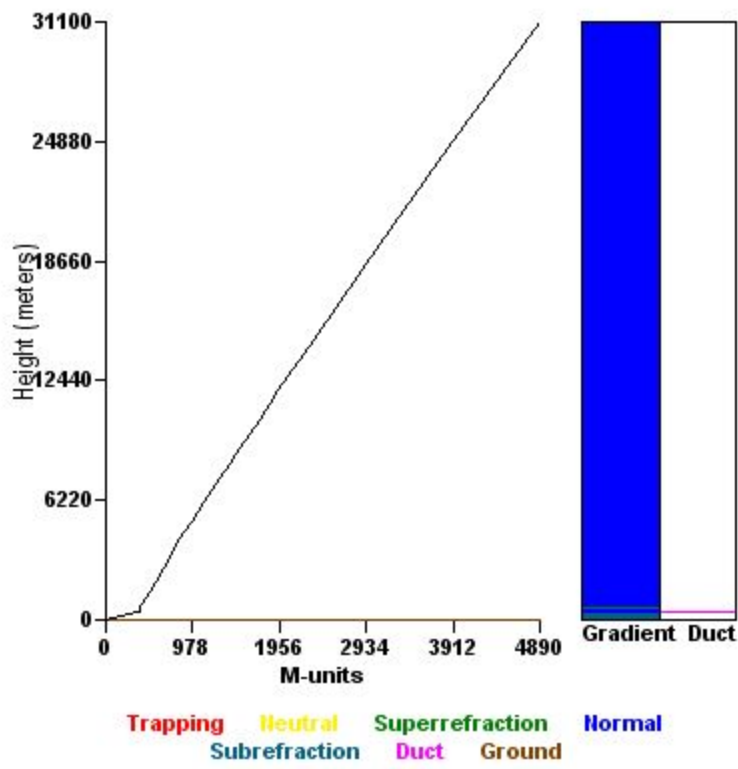


Figure 29. CAAPS Analysis 23 Mar/0100UTC AREPS M-unit graphic.

Center Location: 18°46'48"N / 98°58'48"E - Station: Chiang Mai, Thailand - Date/Time: March
 On bearing: 0 °T - At range: 0.0 km
 Station elevation: 323 meters

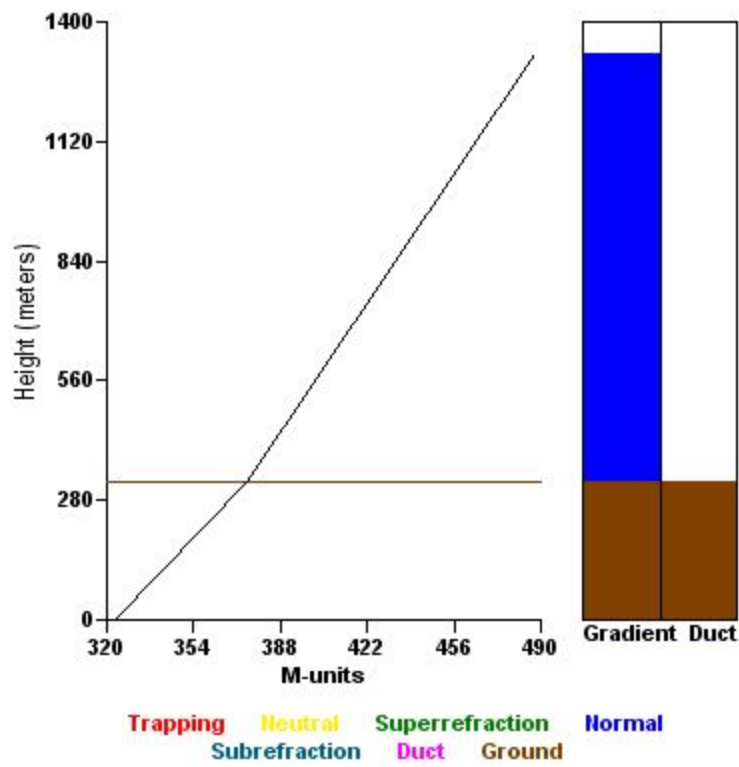


Figure 30. Chiang Mai, Thailand March Climatology AREPS M-unit graphic.

Center Location: 0°N / 0°E - Station: Not specified - Date/Time: Not specified
 On bearing: 0°T - At range: 0.0 km
 Station elevation: 0 meters

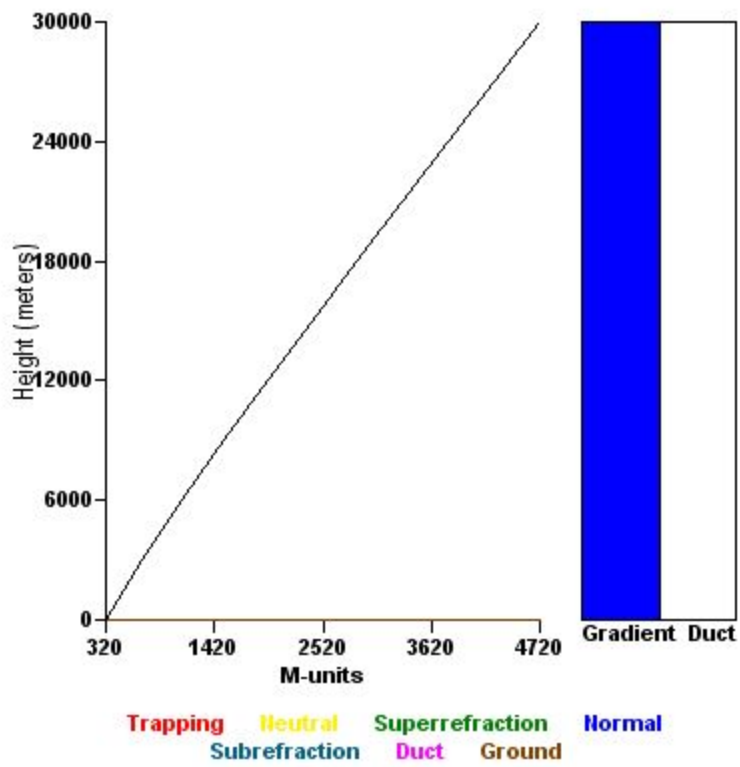


Figure 31. Standard Atmosphere AREPS M-unit graphic.

Table 15. Height/M-unit comparison for all Meteorological data. Height is in meters.

Extraplated		Radiosonde		CAAPS		Clima		Std Atm	
Height	Munit	Height	Munit	Height	Munit	Height	Munit	Height	Munit
0.000	354.126	0.000	331.413	0.000	0.000	0.000	326.615	0.000	326.615
0.006	3640126	6.829	368.340	10.665	368.200	323.000	374.699	3000.000	660.914
0.810	349.816	29.088	395.478	30.350	366.780				
1.218	349.219	37.168	396.508	55.078	370.250				
2.438	348.682	48.160	397.585	89.700	374.210				
4.877	348.304	57.198	397.815						
9.754	348.200	72.878	399.196						
19.507	348.664	78.722	402.878						
39.014	350.268								
78.028	354.161								

V. DISCUSSION

The study of the possible impacts of the propagation environment, including the atmosphere and surface, were based on the application of a propagation model (APM) to collected data. In all APM predictions, the variance of meteorological data; the variance of observed signal data; the accuracy of communication system set-up within AREPS; and the accuracy of terrain input for AREPS were all individually considered. The important ability of APM to take into consideration not only terrain effects, but also horizontal and vertical variations of refractivity conditions make it a robust propagation model for operator use in the description of signal propagation in the lower atmosphere. Additionally, the ability to input *in situ* upper air profiles is a very important feature of AREPS. AREPS is a qualitative TDA for operator use in the evaluation of signal propagation over water, within coastal regions, and over land. Specifically for predictions of communication system signal propagation over land, the TDA should be used in conjunction with manufacturer link budget estimators and as a tool for the network administrator in the evaluation of atmospheric property effects during link set-up and planning.

As noted previously, Barrios et al. (2006) conducted an APM validation study for low altitude signal propagation over land with a *mobile* receiver and varying signal propagation distances. The Barrios et al. (2006) study found up to a 29.9 dBm APM RMS error between the predicted and observed. This study also showed an APM received power prediction error; however approximately half that of Barrios et al. (2006). Further study and expansion of the AREPS communications system set-up allowances and limitations will mitigate a portion of the error found between predicted and observed signal data. Recommend network administrators and/or operators contact SPAWAR (<http://areps.spawar.navy.mil>) prior to deployment for proper AREPS system set-up if considering use of the “user defined” system set-up within the Communication Editor subroutine. Given multiple days of testing and measurements, an operator can also adjust or tune the receiver sensitivity, within the Communications Editor, to effectively zero-out

the consistent over-prediction, and focus on the isolated differences between predicted and measured signal strength and possible impacts.

Barrios et al. (2006) also concluded that refractivity conditions had “little effect of statistical significance” and that terrain resolution and elevation had a greater effect. This research also found negligible statistical significance of refractivity conditions, even though *in situ* meteorological data captured non-standard refractivity gradients. Ground meteorological measurements observed atmosphere conditions creating a strong, shallow ducting layer during the March testing period. March radiosonde measurements also observed a daily, early-day temperature inversion with subsidence at height, creating conditions for the presence of surface and elevated ducting layers. May radiosonde soundings showed daily atmospheric fluctuations during the monsoonal transition season that must be acknowledged and considered for potential non-standard refractivity gradients.

In this study, *in situ* atmospheric variables, when statistically compared to fluctuations in the observed received power showed inconsistent correlations. Consequently, no identifiable linear relationship of atmospheric variables or refractivity gradients and observed signal strength appeared at the operating wavelength and distance. Although the observed atmospheric conditions were found not to affect the studied signal wave length, operators must consider anomalous propagation conditions if operating RADARS and equipment at shorter or longer wave lengths. The ducting and trapping of the transmission signal is frequency dependent and directly related to duct depth. Degradation of the signal resulted from variables other than the atmosphere and local refractivity conditions. Topics for future study should include environmental effects from vegetation, varied terrain features, and urban development. Future research should measure incoming solar radiation and model against external and internal equipment and circuit board temperatures to find any significant relationship between heating of the equipment and degradation of its operation over time.

The primary focus of the study was to get meteorology impacts accounted for, from a test and operational perspective. Hence, five different meteorological data sources were used to create APM input refractivity conditions and for side-by-side comparison.

Large variations existed in the vertical resolution of each input and subsequent refractivity profiles. Little, almost negligible, variation existed in the predicted signal strength values. Observed *in situ* meteorological data is always a goal asset to have and undoubtedly increases situational awareness. This research shows that absent of *in situ* weather measurements, the CAAPS analysis and forecast fields within a data sparse environment gave an excellent approximate understanding of the lower atmosphere for use within a TDA. Climatology and standard atmosphere profiles were, to a much lesser degree, also a reasonable approximation of the environment for use within the TDA when operating at SHF wavelengths and the defined distances. Future research examining different configurations of CAAPS with varying vertical resolution is recommended. Use of accurate CAAPS analysis fields removes the need for personnel downrange measuring the *in situ* environment.

This research shows the viability of surface measurement profile extrapolation in the lowest level of the boundary layer over land. The extrapolated profiles can be used to append to the bottom of an upper air soundings or CAAPS model fields for accuracy of measurements within the bottom 10% of the boundary layer. Operators already use a similar process to capture the evaporation duct over water.

Finally, this research, which was based on rigorous application of atmosphere data and propagation models, shows that it is not the atmosphere impact on propagation that influenced the transmission. Instead, it was shown that the radiation heating of surfaces remains as the likely factor to impact the transmission signal and equipment.

THIS PAGE INTENTIONALLY LEFT BLANK

LIST OF REFERENCES

- Alexander, Bruce, 2005: *802.11 Wireless Network Site Surveying and Installation*. CISCO Press, 432 pp.
- Atkinson, B.W., J.-G. Li, and R.S. Plant, 2000: Numerical Modeling of the Propagation Environment in the Atmospheric Boundary Layer over the Persian Gulf. *Journal of Applied Meteorology*, **40**, 586-603.
- Babin, S.M., 1995: Surface Duct Height Distributions for Wallops Island Virginia, 1985-1994. *Journal of Applied Meteorology*, **35**, 86-93.
- Barrios, A.E., 2003: Considerations in the Development of the Advanced Propagation Model (APM) for U.S. Navy Applications. Proceedings *IEEE Conference on Radar*, 77-82.
- Barrios, A.E., K.A. Anderson, and G.E. Lindem, 2006: Low Altitude Propagation Effects – A Validation of the Advanced Propagation Model (APM) for Mobile Radio Applications. *IEEE Transactions on Antennas and Propagation*, **54**, 2869-2877.
- Burke, S.D and W.T. Thompson, 1996: Mesoscale Modeling of Summertime Refractive Conditions in the Southern California Bight. *Journal of Applied Meteorology*, **36**, 22-31.
- COASTS Program, Naval Postgraduate School, April 24, 2007: COASTS Concept of Operations 2007, Monterey, CA 98 pp.
- Davidson, K.L., 2003: *Assessment of Atmospheric Factors in EM/EO Propagation*, Course Notes, Department of Meteorology, Naval Postgraduate School, Monterey, California.
- Freeman, Roger L., 1998: *Telecommunications Transmission Handbook*. Wiley-Interscience, 4th Edition, 1232 pp.
- Freeman, Roger L., 1999: *Fundamentals of Telecommunication*. Wiley-Interscience, 1st Edition, 676 pp.
- Goldhirsh, J., D. Dockery, and J. Meyer, 1994: Three years of C band signal measurements for overwater, line-of-sight links in the mid-Atlantic coast 2. Meteorological aspects of sustained deep fades. *Radio Science*, **29**, 1433-1447.
- Miller, C.R., 2006: Statistical Analysis of Wireless Networks: Predicting Performance in Multiple Environments. M.S. Thesis, Dept. of Operations Research, Naval Postgraduate School, 56 pp.

Moltzan, Terry, 2005: Design and Analysis of a Wireless Telemetry System Utilizing IEEE 802.16. M.S. Project, Dept. of ECE, Montana State University, 52 pp.

National Imagery and Mapping Agency, 23 May, 2000: Performance Specification Digital Terrain Elevation Data (DTED, MIL-PRF-89020B), 45 pp.

Patterson, W.L., 2007: Advanced Refractive Effects Prediction System (AREPS). Proceedings *IEEE Conference on Radar*, 891-895.

Space and Naval Warfare Systems Center, San Diego, Atmospheric Propagation Branch (2858) Branch Overview, 2005: Our Technology Overview, January 2005, 2 pp.

Space and Naval Warfare Systems Center, San Diego, Atmospheric Propagation Branch (2858), 2006: Statement of Functionality (SOF) for Advanced Refractive Effects Prediction System, Document Version 3.6, 18 December 2006, 4 pp.

Thompson, R.A., D. Tipper, P. Krishnamurthy, J. Kabara, 2006: *The Physical Layer of Communications Systems*. Artech House Publishers, 876 pp.

INITIAL DISTRIBUTION LIST

1. Defense Technical Information Center
Ft. Belvoir, Virginia
2. Dudley Knox Library
Naval Postgraduate School
Monterey, California
3. Dr. Ken Davidson
Naval Postgraduate School
Monterey, California
4. LtCol Karl Pfeiffer
Naval Postgraduate School
Monterey, California
5. Mr. Jim Ehlert
Naval Postgraduate School
Monterey, California
6. Mr. Ed Fisher
Naval Postgraduate School
Monterey, California
7. Ms. Rite Painter
Naval Postgraduate School
Monterey, California
8. SPAWAR Systems Center, San Diego
Attn: Amalia Barrios
Atmospheric Propagation Branch, Code 5548
San Diego, California
9. CO, FNMOC
Monterey, California
10. CAPT A. Brown
PMW-120
San Diego, California
11. Commanding Officer
Navy Information Operations Command, Suitland (NIOC-S)
Attn: Mr. Kato
Washington, DC